Serial Assembly of Microstructures

by Subramaniam Venkatraman

Research Project

Submitted to the Department of Electrical Engineering and Computer Sciences, University of California at Berkeley, in partial satisfaction of the requirements for the degree of **Master of Science, Plan II**.

Approval for the Report and Comprehensive Examination:

Committee:

Professor Kristofer S. J. Pister
Research Advisor

(Date)

* * * * * * *

Professor Carlo H. Séquin
Second Reader

(Date)

Table of Contents

Abstract

Serial Assembly of Microstructures

by

Subramaniam Venkatraman

Master of Science in Electrical Engineering and Computer Science
University of California, Berkeley
Professor Kristofer S.J. Pister, Research Advisor

This thesis presents serial pick and place assembly of microstructures, fabricated in a simple single mask SOI process, as an approach for the manufacture of complicated microstructures. Two techniques for pick and place microassembly and design of microparts which can be used with either of these two assembly approaches are presented. The techniques are designed to be simple and robust so that they can be extended to an automated assembly-line style manufacturing approach. Distinctive aspects of this work are the assembly of microparts into mechanically rigid sockets and the low contact resistance of the assemblies. Out-of-plane motion of assembled microstructures, assembly of hybrid microsystems and other applications of this assembly process are also discussed.

As another example of serial assembly, initial work is demonstrated towards the realization of a silicon robot which can extrude a strut and climb along it. A silicon spinneret is demonstrated which can assemble together silicon connectors to form a silicon strut and then extrude it out. Finally, a few ideas for the future development of such a silicon spider are presented.

1. Introduction

A large number of Micro Electro Mechanical Systems (MEMS) have been realized over the last 20 years. MEMS are today used to sense manifold pressure for controlling fuel flow in fuel injected automobile engines, to sense automobile collisions for airbag deployment, for projection displays using digital micromirror devices, and as FBARs in cellular phones, to name just a few of the devices available commercially.

Significant parts of MEMS processes have been borrowed from Integrated Circuit (IC) fabrication processes which are inherently limited to planar substrates. Three dimensional micro-fabrication has been developed but has typically been limited to a small number of stacked layers which are independently patterned. While this limitation has not strongly limited IC fabrication, mechanical systems are often inherently non-planar. Hence the fabrication technique used restricts the design space of devices which can be created.

One way to achieve fundamentally new micromechanical devices is to rethink the manufacturing process. What if we move away from the idea of fabricating the entire device using IC style fabrication techniques and instead move towards an assembly-line manufacturing technique? We lose the economics of scale inherent in wafer scale parallel processing which has driven the IC industry, but we gain the ability to make significantly more complicated and more truly 3 dimensional structures.

It is important to realize that a tradeoff is available between process complexity (difficulty of wafer level fabrication) and post process complexity (chip level operations).

Post processing also enables more complex / hybrid devices not easily possible using monolithic fabrication. Such assembled microsystems could have applications in fields like micro-optical bench technologies, tunable RF MEMS components, robotic legs for microrobots and scanning micromirrors. This work attempts to develop an assembly technique which can satisfy the above applications and can be extended to assembly-line style automated manufacturing.

However, a problem arises when we try to scale the idea of robotic assembly to small dimensions as in MEMS. The forces in the microscopic regime scale differently as demonstrated in [1] thus making picking up and placing of parts a difficult task. Moreover, the instrumentation required for assembly needs to be scaled appropriately and achieve sub-micron precision over many centimeters, a difficult task given the presence of forces not significant at the macro-scale like thermal drift.

One way in which researchers have sought to solve the problem of assembly at small scales is to move towards parallel assembly schemes. There are two basic approaches towards parallel assembly [2]. One is based on the massively parallel transfer between wafers of arrays of micro components and is called deterministic parallel microassembly. An example is the chip-to-chip transfer of high aspect (HexSil) polysilicon structures demonstrated in [3]. The other form of parallel assembly utilizes various approaches to orient an initially random array of microparts and is called stochastic parallel microassembly. One example is fluidic self assembly as demonstrated in [4]. Dry

processes which use vibrational and gravitational forces to assemble parts have also been demonstrated in [5].

These processes have demonstrated admirably high yields and hybrid assembly of components with sub-micrometer precision. They are clearly the ideal technique for a number of applications like manufacture of RFIDs [6], assembly of micromirrors on microactuators [7] etc. However there are limits to which such processes can be extended and they cannot be used to build highly complex, three dimensional, actuated microstructures.

Another approach towards assembly involves folding of surface micromachined parts to create vertical structures. Rotation of surface micromachined parts on hinges to form three dimensional structures was first demonstrated in [8]. Plastic deformation assembly techniques [9], and assembly using surface tension forces [10] also offer methods to construct three dimensional microstructures. However, in all these cases the assembled devices are constrained to remain in close proximity to where they were fabricated. Moreover, the fabrication is limited to thin film substrates and is difficult to extend to high aspect ratio processes.

A more general, directed pick and place microassembly approach enables the integration of micro-components fabricated in several different processes, thus moving closer to the assembly-line ideal. Very impressive assembled micro gears with bushing tolerances of 0.25μm were demonstrated in [11]. More recently, pick and place microassembly of

surface micromachined parts has been demonstrated in [12]. Assembly of 100 micron size blocks has been demonstrated using adhesives like molten wax and ortho tweezers as shown in [13]. An extensive development of an SOI based automated pick and place microassembly system has been demonstrated in [14].

None of these systems demonstrate the ability to assemble parts in rigid sockets or to interface assembled parts to in-plane actuators as is demonstrated in this thesis. The ability of such assembled systems to create complicated out-of-plane actuation is leveraged in this work. This ability is essential for a number of applications, especially those involving microrobots and micromirrors. Moreover, earlier systems require the use of large and expensive robotic arms to carry out the assembly as opposed to the passive systems demonstrated in this work. The simplicity of this passive approach is essential for automating this system to achieve high-speed automated microassembly.

Thus a pick and place assembly technique for parts fabricated in a single mask process on a Silicon on Insulator (SOI) wafer has been developed in this work. This assembly technique is optimized for manufacture of out-of-plane actuated microstructures. The microparts are designed to be modular so that functionality can be added or dropped depending on the application.

In an attempt to take the idea of assembly further, planar self assembly of a silicon strut is explored. The long term goal of this project is to develop a robotic spider which can extrude a silicon strut and then climb along it. As a first step towards this goal, a silicon

spinneret is demonstrated. Spinnerets are tubular structures from which spiders and certain insect larvae, such as silkworms, secrete the silk threads from which they form webs or cocoons. The system envisioned here extrudes a silicon 'thread' by assembling together silicon connectors using an electrostatic inchworm motor. Some new ideas on electrostatic inchworm motors are also presented which help to make this system possible.

The goal of this thesis is to describe the various design choices and tradeoffs available while designing a serial microassembly system. Various approaches used by our group and others are discussed and their pros and cons analyzed. This thesis is a compilation of the design choices we made and can be considered a guide for someone wishing to design a directed microassembly system.

2. Connectors and Sockets

For pick and place microassembly, it is essential to develop parts (called connectors) which can be picked up and parts (called sockets) into which these connectors can be assembled. Conventional types of fasteners like screws and nuts are not suitable in microassembly because of their complicated structure and motion. The scaling of forces at the micro scale [1] makes the use of conventional fasteners even more difficult. A good way to approach the problem is to think of redesigning LEGO® to work at the micro scale given the constraint that the parts are limited to two and half dimensions. This implies that parts of different shapes and sizes can be designed in two dimensions and these parts all have the same thickness. Given the ability to assemble parts oriented perpendicular to the chip, constraints along all three axes can be applied.

Since macro scale fasteners are not appropriate for use in micromechanical systems, it is

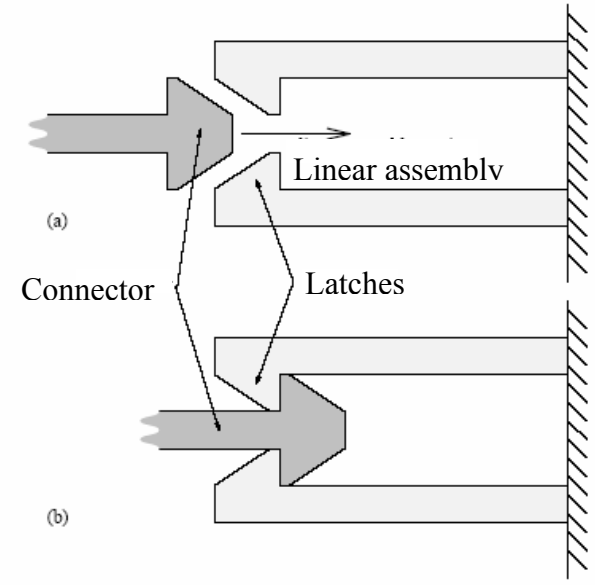

Figure 1: Snap fasteners for microassembly. Figure courtesy of [15]

necessary to come up with new connectors and sockets. Snap fasteners are found to be useful for assembly at the micro domain [15]. A snap fastener consists of a mating pair of a connector and flexible latches (Figure 1). In its disengaged state, connector and latches can move freely with respect to each other. To engage the device, the connector is moved along a straight line towards the latches as depicted in Figure 1a, such that the connector comes in sliding contact with the latches, causing them to bend outward, until the anchor is fully inside the latches. The following properties of snap fasteners make them useful:

- Assembly is simpler than with screws or nuts, as only a linear motion is required to engage the components.
- Assembly is robust, i.e. small errors in the relative position of connector and latches are corrected automatically by their chamfered surfaces.
- The force required to engage the fastener can be chosen over a wide range depending on the shape and size of the device.
- The force to engage can be made much smaller than the force to disengage (motion diode).

Simple calculations to calculate the forces required to engage and disengage snap fasteners are presented in [15]. One of the major requirements is to ensure sliding contact of the faces during assembly. When the two faces come in contact with each other and are being pushed with respect to each other, sticking occurs when the tangential force F_t is less than the frictional force F_r. To avoid sticking, it is needed to ensure that

$$F_t > F_r$$
$$F\sin(\theta) > \mu F\cos(\theta)$$
$$\tan(\theta) > \mu$$

where θ is the angle on the assembling face of the snap fastener and F is the force applied. More generally, θ is the minimum angle of a chamfered face to ensure that the two objects will slip on contact instead of sticking. Assuming a coefficient of friction of 3, (typical value expected when using a self assembled monolayer coating is 0.3) we get θ to be 71.5^{o}. In reality, the coefficient of friction is expected to be lower, so smaller chamfer angles can be used.

It is instructive to compare the design requirements of these parts to those designed for self assembly. In the case of self assembly, the system has to be designed such that the parts try to reach a local energy minimum. If this approach is applied here, it is obvious that the energy taken to assemble and disassemble parts is equal. Therefore, the figure of merit in a directed assembly case is that the force taken to assemble parts be significantly lower than the force taken to disassemble parts. Hence this device is referred to as a 'motion diode'.

One of the first design decisions to be made was to decide on the fabrication process to use. A single mask process on Silicon on Insulator (SOI) wafers was chosen and the reasoning behind that decision is provided below.

2.1. Processing

Deep reactive ion etching into Silicon on Insulator (SOI) wafers has become a popular method for building high-performance MEMS structures. This is primarily due to the need for very flat and smooth structures for optical applications, as well as due to the

desire for large deflections and large actuation forces available using high aspect-ratio micromachining. SOI MEMS provide the ability to generate high aspect-ratio flexures and actuators with the favorable material properties of single-crystal silicon. One of the biggest remaining obstacles in SOI MEMS is the lack of out-of-plane motion [16].

In contrast, surface micromachining incorporates multiple structural layers, offering three primary benefits over SOI micromachining in the design of micromechanical systems:

1) Structures can be folded up out of plane, enabling microsystems to move both in and out of the plane of the chip

2) Multiple layers can be used to keep structures such as gears, motors, and other moving structures from moving in undesired directions

3) Electrical wiring can be kept compact by using multiple routing layers.

Out-of-plane motion of SOI structures has been achieved in a few cases using complicated fabrication processes. In [16], a 4 mask process with timed etches was used to achieve 2 DOF micromirrors. In [17], a complex five mask fabrication process that combined two polysilicon structural layers with thick SOI structures and a backside substrate etch was used to develop robotic leg motion. Assembly of structures fabricated in a simple single mask SOI process provides an interesting alternative to such complicated fabrication processes to achieve similar performance. Hence a single mask SOI fabrication process was used in our work. The major advantages of this process are its simplicity and high fabrication yield. The entire process has been run in the Berkeley

Microlab (from mask making to fabrication to assembly) in less than 30 hours. Details of the fabrication process are provided in [18].

The fabrication process imposes a number of constraints on the design of the microassembly system. A single mask SOI process was used on a wafer with a 20μm thick device layer. The oxide layer was 5μm thick for reasons explained later. The lithography used provides a minimum beam width of 2μm and a minimum gap width of 2μm. These dimensions formed the important constraints in designing the connectors and sockets. The precision of the stages used for assembly added a requirement that the parts self-center during assembly to ensure a sub-micron final assembly tolerance while using stages with around 10μm precision.

2.2. Connectors

The assembly of connectors is based on a careful choice of forces. For the assembly to proceed as planned, it is essential to ensure that the force with which the gripper grips the connector is greater than the insertion force (force required to assemble a connector into a socket). It is further required that the pullout force (force needed to pull out a connector after assembly) be greater than the force with which the gripper holds the connector. This careful choice of forces is essential since electrostatic forces, stiction etc. can show large variations from assembly to assembly.

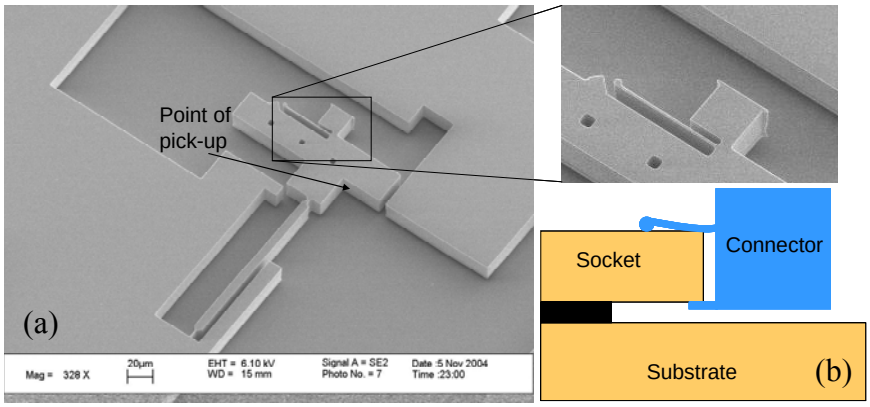

Figure 2: Simple connector design (a) SEM of connector as fabricated (b) Schematic of assembled connector

2.2.1. Spring loaded Connectors

The connector was initially designed to interface with a socket such that a small wedge is stuck into the 5µm gap below the device layer on the socket. The connectors are designed to be first lowered to the substrate and then pushed along the substrate to assemble into sockets. Hence the assembly is termed 'horizontal'. A flexure gets spring loaded against the top surface of the device layer of the socket when assembled as shown in Figure 2b. This ensures that the connector is constrained not to move in the z-axis. The constraint along the X-Y axis is provided by the socket. However a problem was discovered with this design due to the fabrication process used. The SOI wafers are fabricated such that the device layer has a variance in width of +/- 5µm around 20µm. Since the connector is designed to interface to this 20µm thick device layer, it is difficult to design such that the connectors work appropriately at process corners. One advantage of this approach is that the connector is not in contact with the substrate so the socket need not be fixed with respect to the substrate.

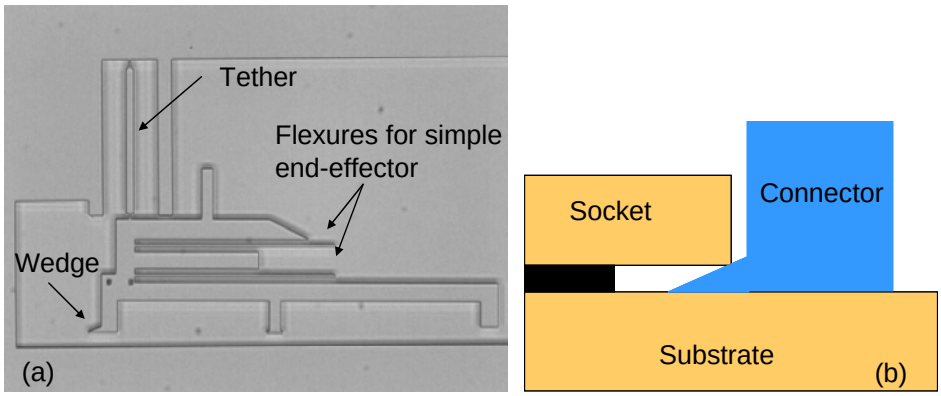

Figure 3: Wedged connector. (a) SEM of connector with wedge to interface with oxide gap (b) Schematic of assembly into socket

2.2.2. Wedged Connectors

It is important to design a connector such that the insertion force and pullout force be independent of device width variations. This problem was solved by realizing that one dimension which had significantly lower variations was the thickness of the oxide layer (thickness of gap below device layer). This thickness is specified to be 5µm with a variation of less than +/-0.2µm. So a modified connector was designed with a long wedge which jammed into the 5µm gap between the device layer and the substrate (Figure 3). This serves the same function of constraining the motion of the connector in the z-axis while significantly easing the assembly process since it can be slid along the substrate during the approach. One problem is that the connector is in direct contact with the substrate so this socket is constrained to be fixed to the substrate. This could limit some designs in applications such as microrobots where it would be useful to have the base of the assembled legs move.

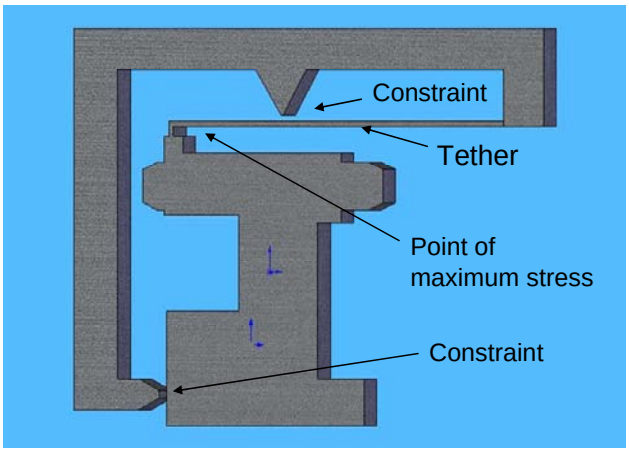

Figure 4: FEA model of tether for stress analysis

2.3. Tethers

Tethers are used to attach the connectors to the device layer until they are picked up. In addition to keeping the parts from sticking to the substrate during the release, they also hold the parts in well-defined locations to aid picking-up of parts. The most important requirements of a tether are to break reliably, at a pre-determined location, with low applied force, and without generating debris.

The tethers were initially designed (Figure 3a) to be broken directly by the orthogripper. After grasping the part, the orthogripper (described in Section 3) would move sideways, thus applying a force on the tether. However it was found that the force required to break the tether was greater than the force required to substantially deflect the orthogripper. When the tether broke, the strain energy stored by the deflection of the orthogripper was sufficient to turn the connector into a projectile. Even in the best case, the connector would shift in the grip of the orthogripper, causing the rotation to not work as well as planned.

One way this problem was solved was by using a second probe tip to break the tethers after the connector had been gripped. The secret to success here was to push the connector against a sidewall and then push against the tether with a probe tip until it fractured. Thus the resultant strain energy stored did not disturb the grip since the sidewall acted to restrain the connector in place. The problem associated with this approach is the introduction of a second micropositioner in the assembly.

A tether with an improved stress concentrator was designed using finite element analysis. The aim was to achieve a stress in excess of 2GPa with an applied force of 200μN with some size constraints. Since the analysis required surfaces in contact and motion along those surfaces, designing to meet the given constraints proved to be difficult. This design is shown in Figure 4. However, when tested it was found that the tether acted as a torsional spring, rotating the part out of plane thus rendering the contacts useless. Hence this approach was abandoned. Most of our assemblies were performed using two probes as described earlier.

2.4. Sockets

Once the connector has been removed from its initial location and rotated 90^{o} out of plane, it is carried to its final location and attached to the socket. An ideal mechanical connector would fuse the connector and the socket into the functional equivalent of a solid piece of silicon. The assembly should provide a strong mechanical connection and a low electrical and thermal resistance. It would be beneficial if the sockets could also provide some degree of self centering to help guide the connectors into them during the

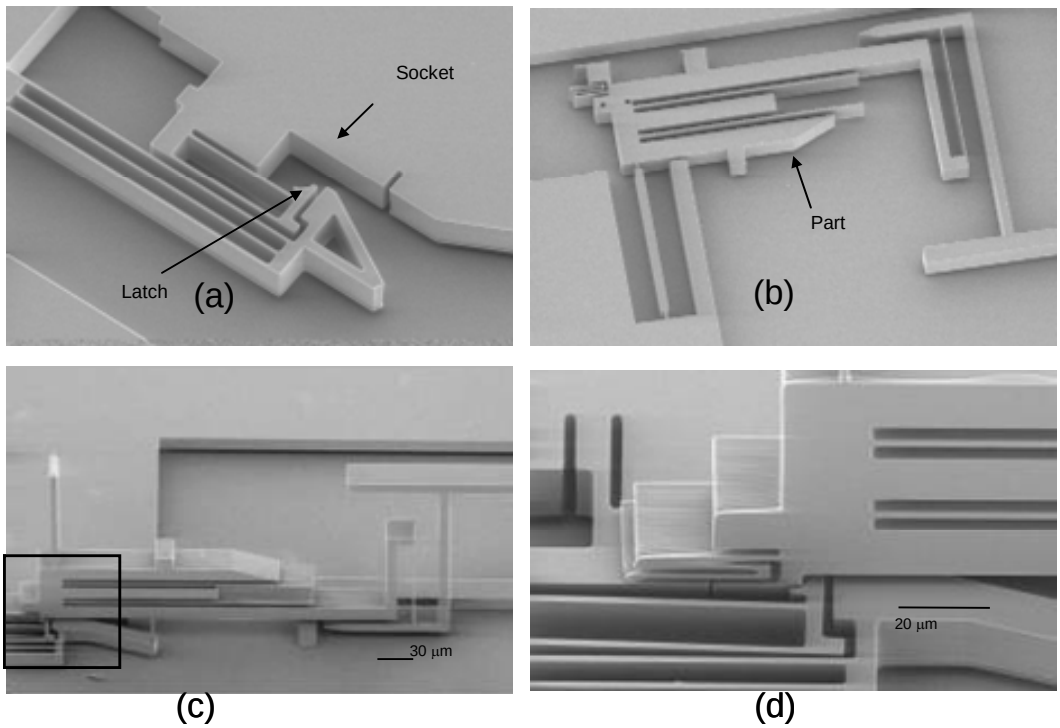

Figure 5: Snap Lock socket and connector. (a) Snap Lock socket (b) Connector (c) Connector assembled into socket (d) Close-up of assembly

assembly. This helps to reduce the positional accuracy requirements on the assembly system. Two kinds of sockets were designed and tested which satisfy the above requirements.

2.4.1. Snap Lock Sockets

As mentioned earlier, the connectors are designed to be lowered to the substrate near the socket and then slid along the substrate into the socket. The snap lock socket consists of a latch-based system suspended by parallel flexures (Figure 5a). The latch has a long ramp which is pushed open by the connector as it is inserted. When the connector is in place, the latch snaps back shut holding the connector in place and preventing motion in plane. In the final state, the flexures of the snap lock are deflected ensuring that that the connector is held with some force. Moreover, the final position of the connector is

defined only by the sidewall of the snap lock and not by the positional accuracy during assembly. The connector design itself prevents motion in the z-axis by interfacing with the device layer (spring loaded or wedged interface as explained in Sections 2.2.1, 2.2.2) at the end of the latch thus ensuring that the connector is constrained in all 6 DOF.

This design suffers from two significant problems. The first stems from its difficulty in handling parts of different thicknesses. A change in the device layer thickness changes the deflection needed by the latch to open and consequently changes the insertion and the pull-out force. The second is that the latch does not strongly resist rotational and torquing motion applied on the connector in the device plane.

As implemented, the snap lock does not provide much resistance to direct pull-out forces either. Testing shows that the pullout force is roughly 65μN (value obtained using a spring-based force gauge) while many of our actuators can apply over 100μN. During operation of the electrostatically-actuated single degree-of-freedom rotation stages (described in Section 4), the parts were seen to shift inside the socket. Clearly, this type of connector doesn't provide a strong enough mechanical connection.

The connectors were then coated with 30nm of gold and then assembled into the sockets to test for electrical conductivity. Since the preload force is small (~30μN) and can vary depending on device thickness of the particular run, it was found that the resistance between the connector and the socket was still in the order of MΩ. This is expected since it is usually found that higher force (many tens of microNewtons) is generally necessary

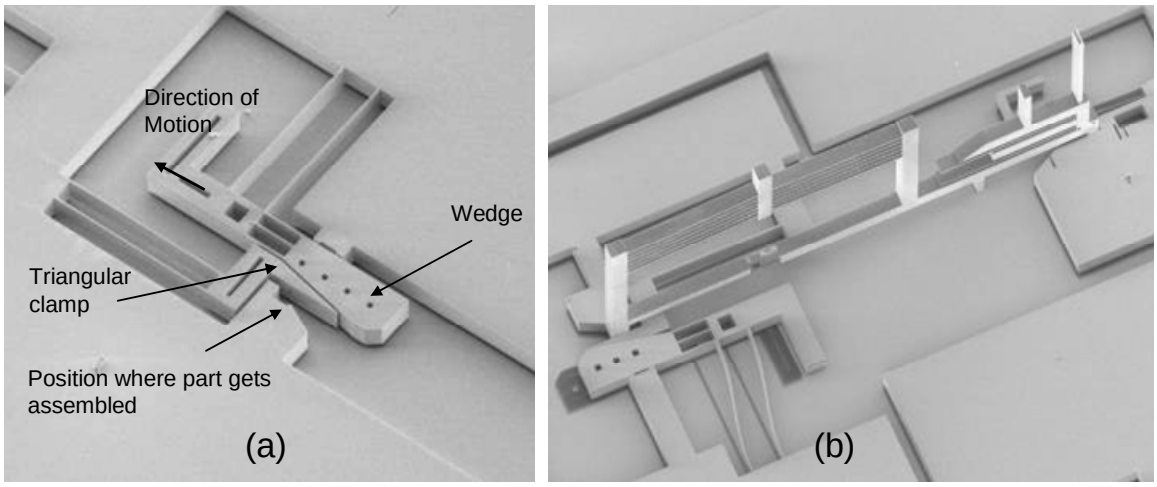

Figure 6: Clamp socket. (a) Clamp as fabricated (b) Clamp after assembly. Shadow from gold deposition shows location of wedge before it was engaged

to generate sufficient number of micro-contacts at the interface to significantly reduce the resistance of the contact [19]. It is possible that a stronger snaplock design usable with rigid end-effectors can show low contact resistances since previous results [19] indicate that the force required for low resistive contact is only around a factor of 2-3 higher.

2.4.2. Clamp Sockets

The clamp socket uses frictional forces to hold the connector in place. It consists of a fixed L-shaped piece which constrains the connector (Figure 6a). A triangular clamp is mounted on a parallel-bar flexure that moves to adjust for the range of thickness of the inserted part. Next to the triangular clamp is a wedge-shaped piece of silicon mounted on a parallel-bar flexure (moving orthogonally to the other parallel-bar flexure) that can slide between the triangular clamp and the rigid device layer. This wedge is used to force the triangular clamp against the inserted part and adjusts for the tolerance in part thickness. This wedge is connected to an L-shaped handle that is pulled with a micromanipulator-mounted probe tip to close the clamp. The clamping force exerted on the inserted part is

limited by the force used to engage the wedge and has been shown to be limited by the strength of the silicon beams connecting the wedge to the handle. In the current design, this is the fracture strength of the three 4μm-wide, 20μm (+/-5μm)-thick, 50μm-long beams.

Assembly of the part into the clamp starts the same way as the snaplock: the part is picked up from the substrate, rotated 90^{o}, and carried to the clamp location. It is then lowered to the substrate and slid horizontally into the clamp. Once the part is roughly in position, the wedge is slid into place with a probe tip, clamping the part firmly into the socket and aligning it to the sidewall of the L shaped part. The ortho-gripper can now be easily removed from the part since the clamping force is on the scale of several milliNewtons while the orthogripper grips with a force on the order of a few tens of microNewtons. By separating the insertion step from the clamping step, the forces required for each step remain independent of one another and can be separated by several orders of magnitude.

The clamp addresses all the major weaknesses of the snap lock socket. The insertion force can be brought down to zero while still providing a ramp to correct for positional errors. The pull out force is measured to be several milliNewtons in all directions as is described in the next section. Thus the clamp provides a mechanically rigid connection as is desired. The only disadvantage of this design is the fact that a second micromanipulator based probe is needed to complete the assembly operation.

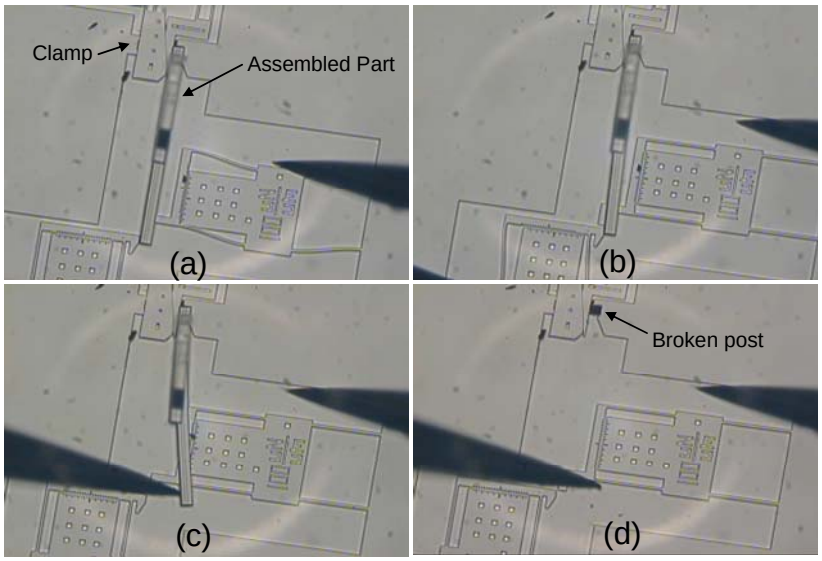

Figure 7: Pullout force test of clamp socket. (a) Pulling straight out with force gauge (b) Pushing sideways with force gauge (c) Pushing directly with probe tip (d) Part breaks

2.5. Clamp Characterization

The clamp socket was designed to provide a rigid mechanical contact with low contact resistance and this was verified by a number of tests.

2.5.1. Force Tests

An initial series of tests was used to verify the pull-out force of the clamp. A connector was assembled into it such that a second leg of the connector could interface to a force

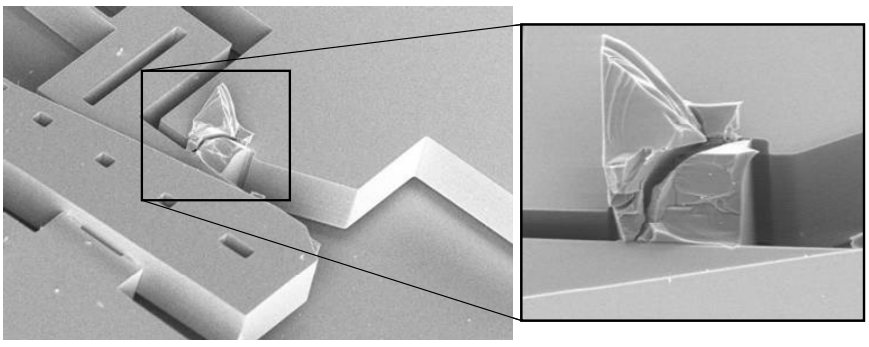

Figure 8: Post of assembled part in clamp after stress fracture

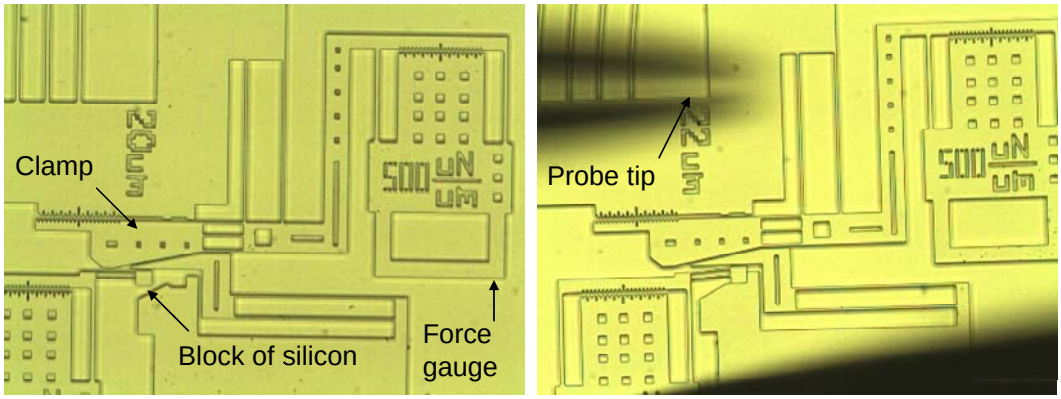

Figure 9: Mechanical characterization of clamps

gauge (Figure 7). The force gauge was pulled using a micromanipulator mounted probe to verify the maximum force that could be applied. Since two orthogonal force gauges are present, a direct pullout force and a torque could be applied on the assembled part. In both cases, the force gauges reached maximum at 2mN without any noticeable motion at the clamp. Then the part was pushed directly with a probe tip. It was seen that the connector broke before the clamp gave way, indicating that the pullout force was greater than the fracture strength of the connector itself (Figure 8). The force required to break the connector by pushing sideways was estimated at 5.4mN by estimating the fracture stress of silicon to be 2GPa.

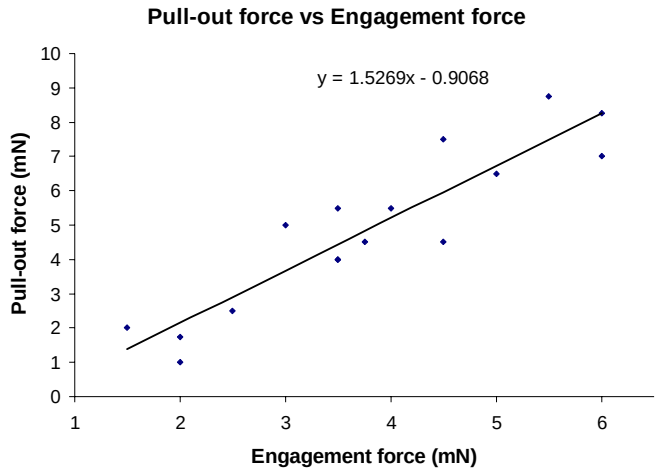

Figure 10: Pullout force vs Engagement force of clamp socket

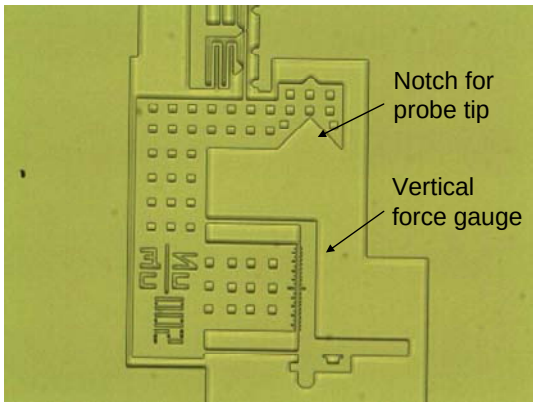

Figure 11: Vertical pull-out force test structure

In a second series of tests, an in-plane block of size 20µm x 20µm x 20µm was suspended by flexures next to the clamp as shown in Figure 9. This was then inserted into the clamp and the clamp was engaged. Using the force gauges present, it was possible to measure the engagement force and its relation to the pullout force required to remove the part. Below a certain engagement force, the part slips back out as expected due to the force exerted by the flexures. Above this threshold, it was found that the pull-out force was proportional to the engagement force as expected (Figure 10). For a maximum engagement force (by directly pushing with the probe tip), it was found that the part stayed securely clamped for a pullout force of up to 12mN. Higher forces could not be measured since the force gauge was designed for a maximum force of 12mN.

To measure the strength of the assembly in the vertical direction, a connector attached to a force gauge was designed which could be picked up and assembled into a clamp (Figure 11). This force gauge was then pulled vertically to measure the vertical pullout force that can be applied on the part (Figure 12). Again it was found that the force gauge displayed a maximum force of 12mN and then broke but did not disturb the assembly of the connector.

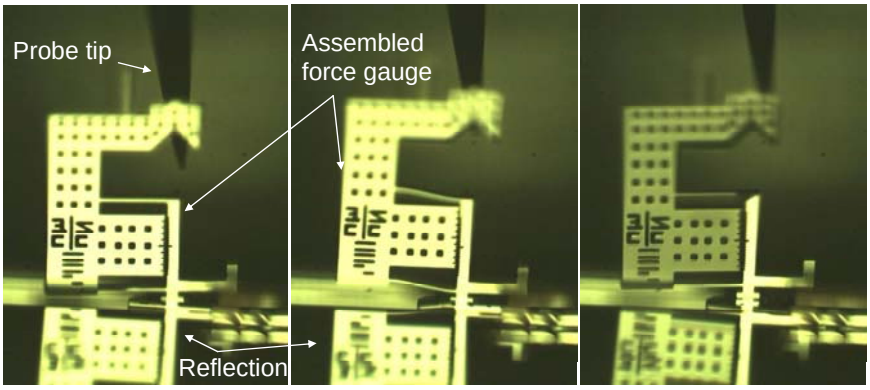

Figure 12: Pullout Force test. a) Test structure is assembled into a clamp and probe tip is brought into position b) Structure is pulled upwards with probe and force exerted measured on force gauge c) After displaying maximum force (12mN) force gauge breaks

The various results are summarized in Table 1. Figure 13 shows the direction in which the forces mentioned in Table 1 are applied.

Insertion force for assembly (1)	0
Minimum force required to engage socket (2)	3mN
Pullout force in direction of assembly (3)	>12mN (high engagement force used)
Pullout force in direction perpendicular to assembly (4)	Part breaks at 5.5mN without affecting the assembly
Pullout force in vertical (out of plane) direction (5)	>12mN (high engagement force used)

Table 1: Characterization of socket in terms of force taken to engage and forces taken to remove part after assembly

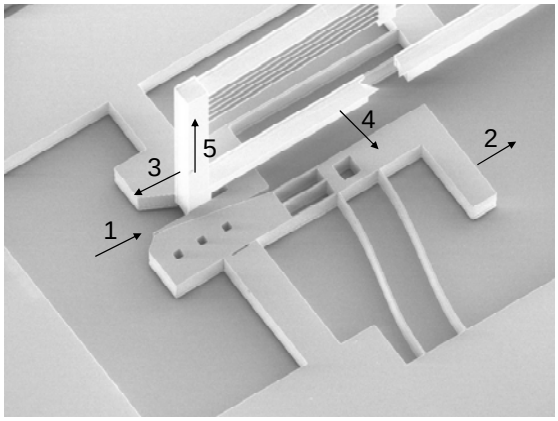

Figure 13: Direction of forces mentioned in Table 1

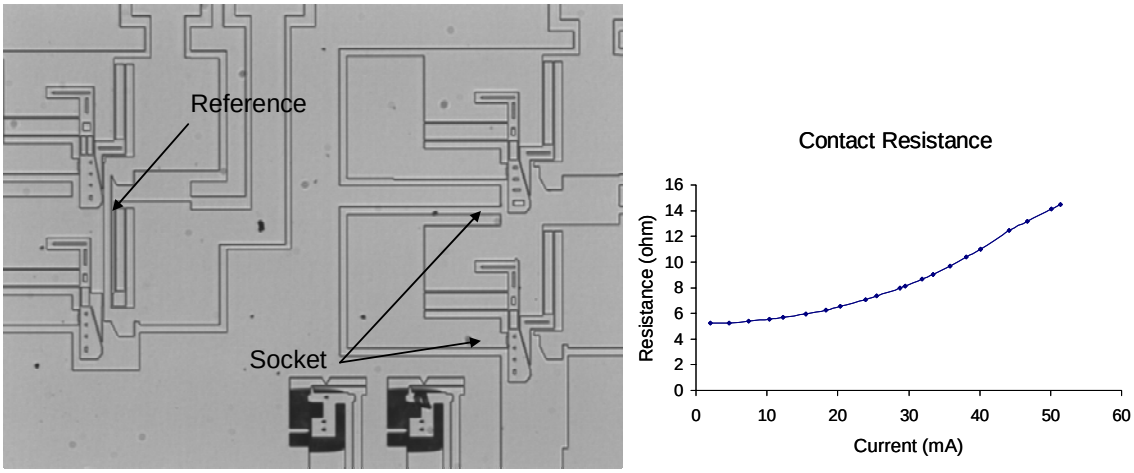

Figure 14: Contact Resistance test. (a) resistance test structure with dummy (b) Variation of contact resistance with current

2.5.2. Contact Resistance Tests

The contact resistance of a part assembled into a clamp is another parameter of interest since a low contact resistance is essential for some applications like vertical thermal actuators (described in Section 4). This was tested with two different structures to yield similar results. In all tests, the entire chip was first released then coated with a thin layer of chromium (6nm) followed by a layer of gold (30nm). These metals are evaporated onto the chip hence are deposited only on the top surfaces of the structures. The 5µm oxide gap ensures that this gold does not lead to shorting of devices to the substrate.

In the first structure, a connector was assembled into two clamps such that it formed an electrical connection between the two (Figure 14). It is ensured that the gold surface on the connector comes in contact with the sidewall of the clamp. Wire bonds are attached to bond pads attached to the two clamps and the resistance between them measured to be about 98.4Ω. However this resistance is the sum of the resistance of the assembled connector, two contacts, bond wire resistance etc. To subtract out these parasitics, an

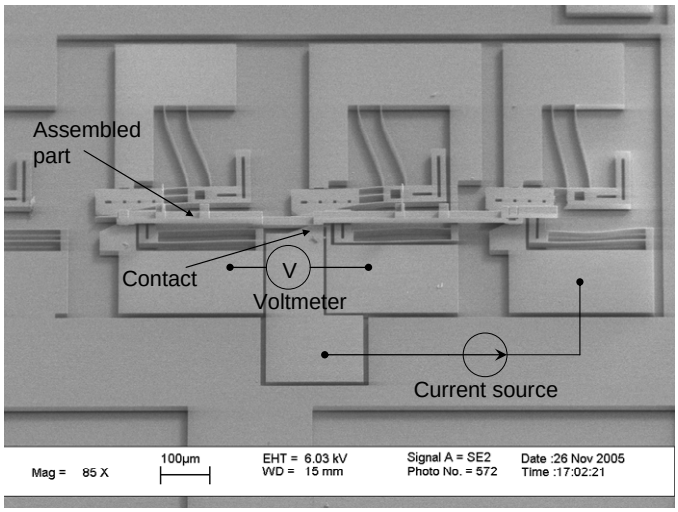

Figure 15: Four point probe test structure

identical structure is fabricated next to it, except that the assembled silicon part is replaced with an in plane silicon part of the same length. Wire bonds are then attached to these clamps and the resistance measured to be 88.0Ω. If designed correctly, this reference resistance can be used to subtract off all the parasitic resistance. The difference then is the sum of two contact resistances. The contact resistance is thus measured to be 5.2Ω. This resistance increases with increasing current and is shown in Figure 14b. One reason for this increase could be the increase in resistance of silicon with increase in temperature due to the heating of the part.

A second generation contact resistance structure was designed based on a four-point probe resistance measurement principle. The socket consists of three clamps with the central clamp attached to two bond pads. A connector with three legs is assembled into the three clamps. The contact resistance of the middle clamp is measured. Current is run from a wire bond, through an anchored pad, through the third contact into the assembled part, through the middle contact to another anchored pad, and out through another wire

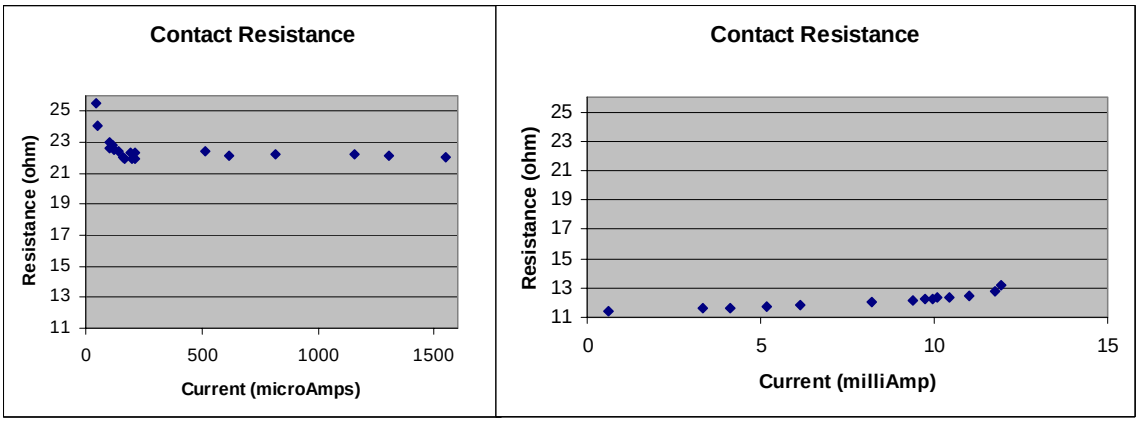

Figure 16: Contact Resistance as a function of current. (a) Initial resistance (b) Resistance after break in

bond. Voltage is measured across the other two pads, i.e. from a wire bond to a pad, across the middle contact, through the other half of the assembled part, and out of the first pad and wire bond. Because no current flows through this portion of the structure, its resistances and that of the first contact do not cause a drop in voltage. The only voltage drop measured is the resistance of the part of the structure where both current is flowing and voltage is being measured, i.e. the central contact. This assembled structure is shown in Figure 15.

A more careful I-V measurement was performed using this device which showed that the contact initially displayed a high resistance which later dropped down to a stable low resistance as the current was increased. This was attributed to localized heating causing the formation of more microscopic contacts and thus lower resistance. These I-V curves (Figure 16) showed a stable resistance of around 12 Ω. This was further verified by directly using an ohmmeter which also gave a value around 10 Ω. A further increase of current caused a sudden increase in resistance which then stayed high even when the

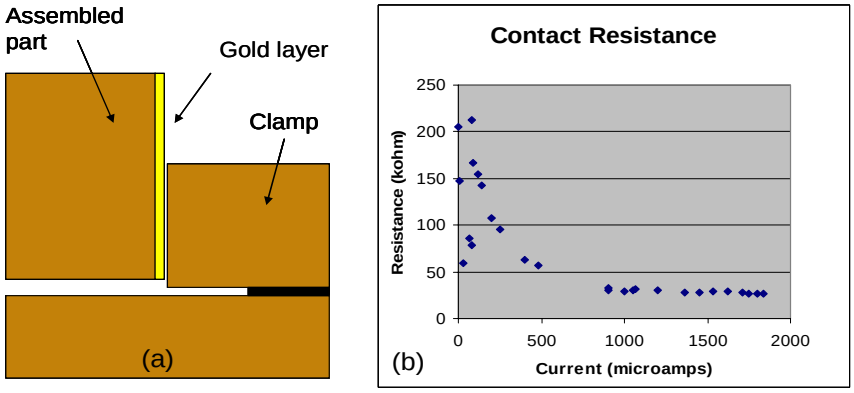

Figure 17: Contact resistance with single gold surface. (a) Schematic of assembly (b) Contact resistance as a function of current

current was decreased. This is probably due to excessive heat generation at the contact causing the gold to melt.

There are two possible mechanisms for contact resistance using gold on the assembled connector. One is that the gold forms a eutectic contact with the silicon on the sidewall. The other is that the gold simply forms a contact with the gold on the top surface of the clamp. To test which of these mechanisms dominate, a second test was performed with the clamp having no evaporated gold on it but the assembled part having gold (Figure 17). In this case the I-V curve obtained is presented in Figure 17(a). The significantly higher resistance of around 28kΩ implies that the gold on the top surface of the clamp plays an essential role in the contact resistance. The high resistance of the clamps in this case (no gold coating) causes significant variations in the measurements. Since the maximum power dissipated at the contact in this case is 90mW, it is possible that the temperature hadn't reached a level high enough to cause eutectic formation. Since only one test of this particular configuration was performed, further tests would be necessary to conclusively determine the nature of the contact.

Thus the clamp socket is demonstrated to provide a strong mechanical connection and a low electrical resistance. Once the connectors and sockets required for microassembly are designed, it is required to design the tools and assembly techniques to interface these connectors to the macroscopic world. This design is presented in the Section 3.

3. Assembly Tools and Techniques

Microassembly of parts less than 10 mm in size requires an infrastructure of tools and microparts, designed to interface with each other and ultimately, with the macroscopic world. 'Design for assembly' is a well-known concept in manufacturing [2]: the assembly process of an aggregate product is streamlined by a clever design of its components (for example, if all components can be assembled without moving or rotating the substrate). This concept is even more important at the microscale due to the difficulty in handling microparts. Tools and techniques developed for microassembly are presented in this section.

A pick-and-place microassembly system typically needs to perform the following set of steps using a microgripper:

- Grip a micropart
- Break the tethers holding the part to the substrate
- Lift and rotate the part out of plane
- Translate it along x, y and z to a second location
- Join it to another micropart and un-grip the part

In this way, out-of-plane 3-D microstructures can be assembled from a set of initially planar microparts.

A similar approach towards pick-and-place microassembly to the one discussed in this thesis has been demonstrated by two other groups; at the University of Toronto [20] and

at Zyvex [14]. The three approaches differ in the fabrication process used, the design of the microparts, the tooling required and the applications towards which they are targeted.

3.1. University of Toronto Approach

The Univ. of Toronto microassembly system [20] makes use of a surface-micromachined microgripper that is solder bonded to a robotic manipulator using a device named the "*contact head*". The contact head is a custom made soldering iron which allows electrical

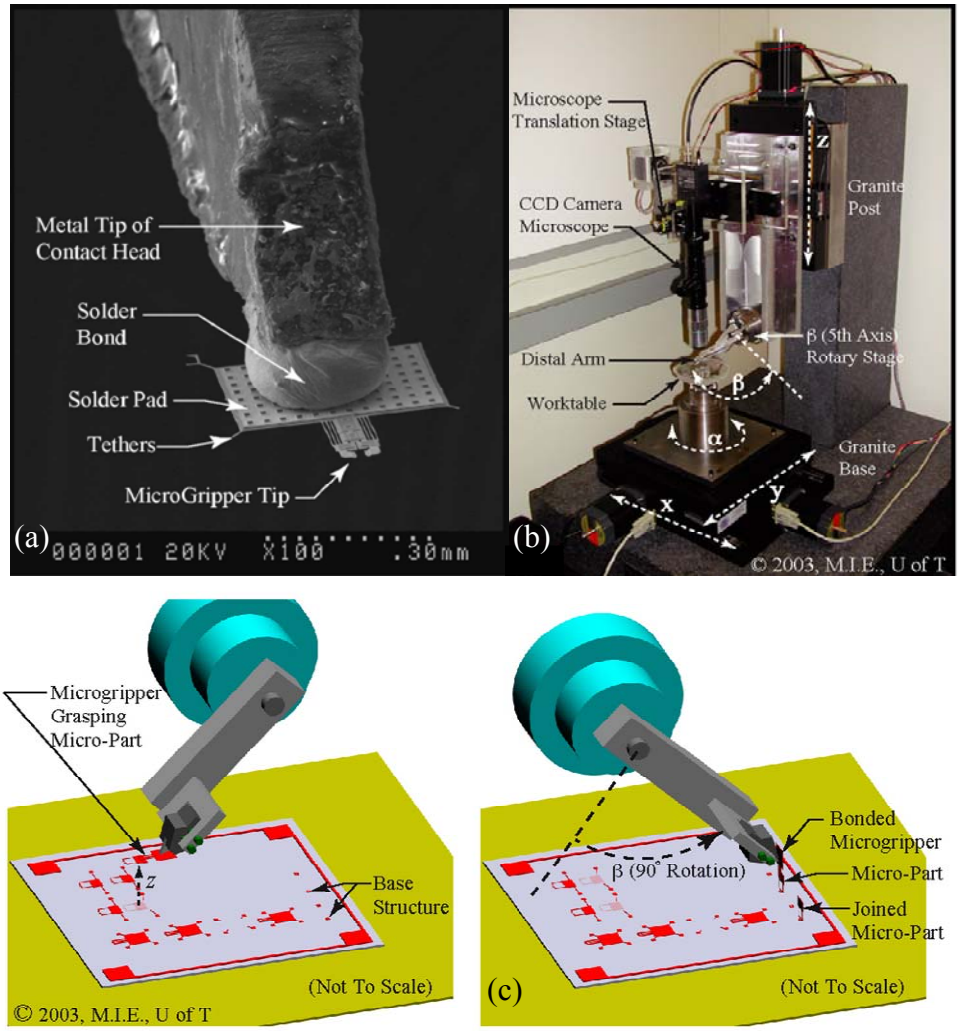

Figure 18: Univ. of Toronto Microassembly Process. (a) Contact head for assembly (b) Robotic Manipulator (c) Principle of assembly. Figure courtesy of [20]

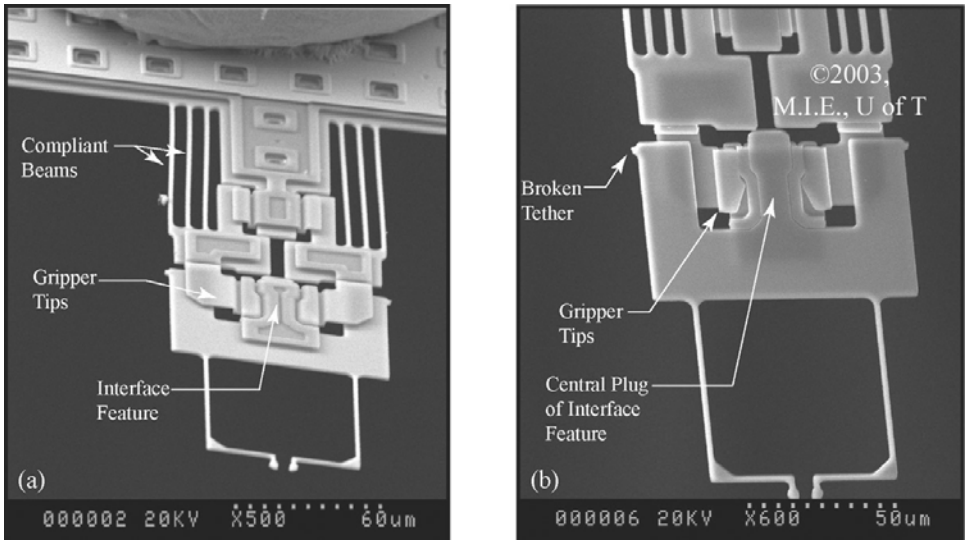

Figure 19: SEM of micropart within the grasp of a microgripper. (a) Top view (b) Bottom view. Figures courtesy of [20]

and mechanical contact between the robotic arm and the microgripper (Figure 18a). The robotic manipulator used has five degrees of freedom (DOF) with translation stages having 0.1μm resolution (Figure 18b). This five DOF station is essential as the micropart is picked up and rotated by 90^{o} so that it is perpendicular to the plane of fabrication, and then assembled. Such a robotic manipulator is large and expensive and would impede the possibility of scaling such a process to assembly-line style microassembly.

The microgripper is designed to be passive and compliant and is fabricated using the PolyMUMPs process (Figure 19). The gripper tips have a 3-D interlocking geometry that secures microparts in all six DOF after they are grasped. This is one of the main advantages of using a multi-layer surface micromachined process as opposed to a single layer process, in that motion of parts relative to the gripper can be restricted in all six dimensions.

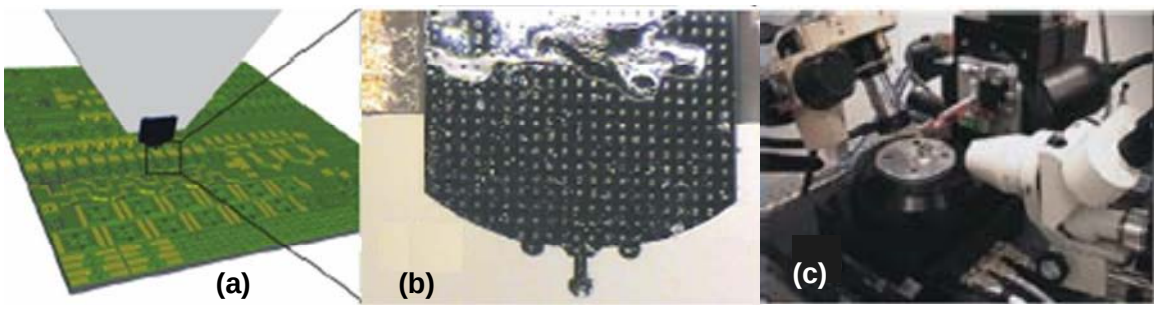

Figure 20: Zyvex Assembly Process. (a, b) Passive rigid end-effector (c) 5 DoF robotic stage. Figures courtesy of [14]

3D microcoil inductors built from up to 6 microparts have been demonstrated in this process as have numerous kinds of connectors and sockets. This process seems suitable to develop electrical applications of microassembly like optical columns for imaging applications, microcoil inductors etc.

3.2. Zyvex Approach

The Zyvex microassembly system [14] uses a passive end-effector, fabricated in a 50 μm thick, single crystal silicon (SCS), DRIE process (Figure 20b). It eliminates the need for any actuated gripping mechanism or even a passive gripping mechanism as shown in the previous case, and instead uses a very rigid passive end-effector to accomplish the micromanipulation tasks. The passive end-effector has several orders of magnitude higher stiffness than compliant grippers and can deliver and tolerate much higher forces both in-plane and out-of-plane.

However, the tradeoff for greater stiffness in the end-effector is the requirement for more complicated microparts which allow the grasping to take place. Moreover the system requires a 5 DOF robotic station to perform the assembly operations. A 3 DOF stage is

used to mount the chip and a 2 DOF arm holds the gripper. This arm performs the crucial 90^{o} rotation required to orient the parts perpendicular to the chip after pick-up.

The rotation actuator is placed in series with the z-axis actuator in both cases described above. Due to this, the mass of the rotation stage must be moved by the z-axis stage. For a macro-scale actuator, this mass will dwarf the mass of the part, dramatically reducing the speed of the robot. Thus the rotation is the cause for a significant part of the assembly time. Currently, Zyvex has demonstrated automated assembly at the rate of about one assembly every 25 seconds. Higher assembly speeds would make this process more useful for industrial production. The rotation also leads to misalignments if the gripper is not well aligned to the robotic arm.

Relatively high speed automated assembly and serial assembly of parts have been demonstrated in this process. Two major products under development are an assembled electron column for a mini SEM (Scanning Electron Microscope) and a mini Mass Spectrometer [21].

3.3. Orthogripper approach

The two approaches described earlier require the use of large and expensive robotic arms to carry out the assembly as opposed to the passive, MEMS based system presented in this section. The simplicity of our approach is important to achieve the goal of high speed automated microassembly. This approach, along with the design of some of the microparts, was developed along with M.E. Last [18].

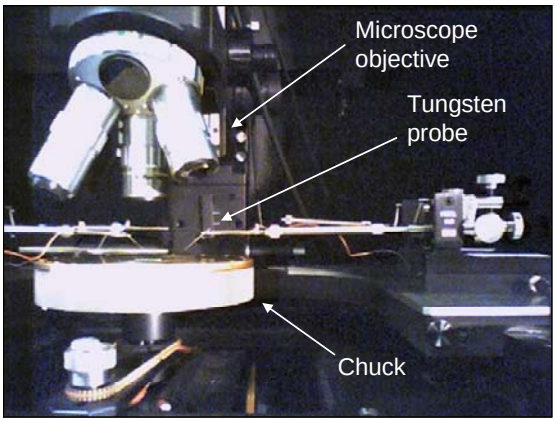

Figure 21: 3-axis manual micromanipulator stage

In contrast to the two previous pick-and-place approaches, the approaches in this work were designed to use only micro positioners found in most MEMS laboratories. This led to the additional constraint that we were restricted to using a thumb screw operated, three axis micropositioner for assembly operations. This consists of a manual probe station from 'The Micromanipulator Company' along with the 110/210 three-axis X-Y-Z manipulators with 10µm of precision.

The use of a three-axis manipulators resulted in the requirement that the crucial 90^{o} rotation (to orient parts perpendicular to the chip after pick-up) be integrated with the MEMS microgripper. The 10µm precision of the stages added a requirement that the parts self-center during assembly to ensure a sub-micron final assembly tolerance. Ease of use led to a final requirement that the microgripper be passive. These requirements also make the system more amenable to automation, if desired in the future.

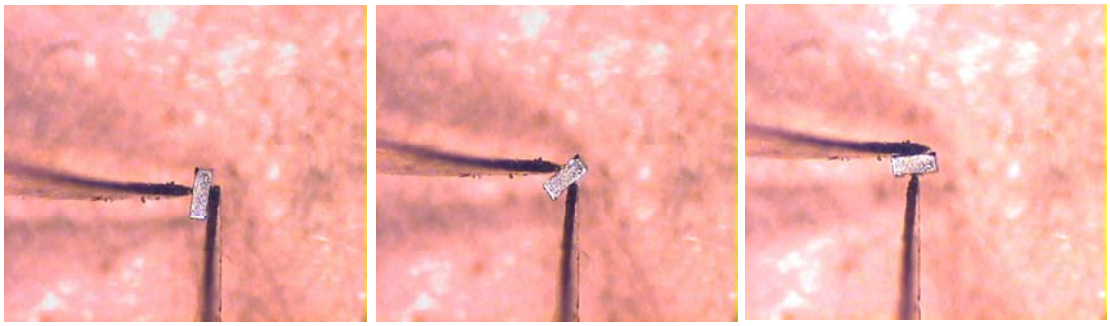

Figure 22: Ortho tweezer rotating a block. Figures courtesy Eiji Shimada.

3.3.1. Orthogripper Design

In [22], dexterous manipulation of sub-millimeter size rigid blocks using two 1 DOF fingers and an XYZ micro-positioning stage was demonstrated. The fingers are arranged perpendicular to each other hence the name 'ortho-tweezers'. This perpendicular configuration makes it possible to rotate a micro-component by controlling the direction of motion of each finger separately. The fingers are several millimeters in size and are independently driven using piezoelectric actuators. Pick and place operations of 100µm blocks have also been demonstrated (Figure 23).

This same ortho-tweezer approach can be scaled down and used as a microgripper. Thus a gripper can be equipped with the ability to pick and place parts and also with the ability to rotate parts by 90^{o} before assembly, removing the need for an external rotation stage.

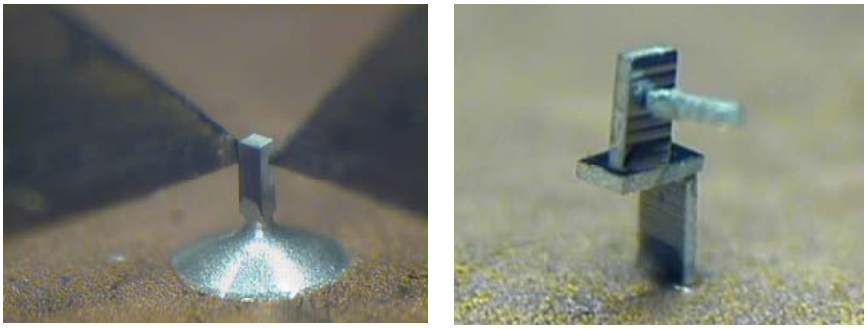

Figure 23: Pick and place operations on blocks with assembly using molten glue or UV cured epoxy. Pictures courtesy Eiji Shimada.

The orthogripper was designed to satisfy the following criteria:

- Provide an interface between the macro and micro world
- grip the part firmly
- be strong enough to break the tether holding the part to the chip
- reliably rotate the part by exactly 90^{o}
- and release the part once it has been placed in its socket

Since the assembly process requires the tool to perform only one well defined motion (pick up and rotate a part), a passive device is sufficient. Two perpendicular spring loaded fingers are used to interact with the part. Instead of being actively actuated as in [13], the springs are pre-loaded while positioning the gripper. As the part is lifted up, the energy stored in the springs is used to rotate the part. In order to perform an accurate rotation motion, the net torque on the part should always be in the correct direction (this case clockwise). Moreover, the gripper must stably hold the part in the fully rotated position. The principle of operation is demonstrated in (Figure 24)

a) The orthogripper is lowered on the part after positioning accurately.
b) The vertical spring is preloaded as it is pushed down against the part. The small wedge is positioned below the part in the gap between the device layer and the substrate. The small beam to its left serves as a height indicator since it deflects when it touches the substrate. This deflection can be observed as a change in color and is used to position the orthogripper in the z-axis.

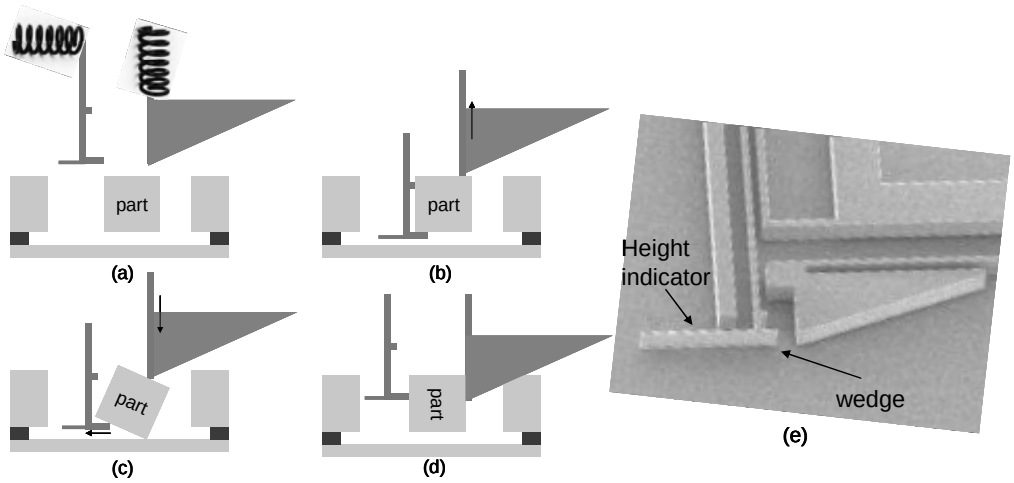

Figure 24: Principle of operation of Ortho-gripper

c) The part is then pushed into the plane to break the tether (or the tether is broken with a probe tip while the part is grasped by the gripper). As the gripper is lifted up, the part begins to rotate as the springs are unloaded.

d) The part completes 90^{o} of rotation and is held in place by frictional forces

The requirement in (b) necessitates the use of a thick oxide layer (5μm thickness is used in our process) between the device layer and the substrate. This is due to the fact that the 2μm thick wedge has to fit in the gap between the part and the substrate to ensure a proper rotation of the part. The other option is to use a backside etch hole under the part. However, this necessitates the use of a second mask and a significant increase in fabrication complexity. This approach was tested anyway and yielded expected results.

The torque applied on the part is calculated by considering the forces applied by the two spring loaded fingers on the part, the distance between the fingers and the axis of rotation (Figure 24e). There are three parameters which can be varied to ensure this: the ratio of

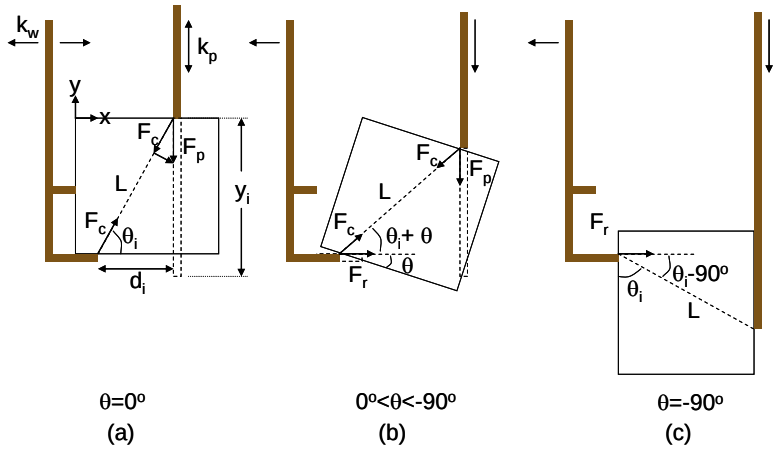

Figure 25: Free body diagram of the orthogripper

spring constants of the two fingers, the initial displacement of the pre-loaded finger, and the initial angle between the contact points of the two fingers. The force exerted by the two fingers is constantly varying during the rotation. Moreover, the moment arm used to calculate the torques is also constantly varying during the rotation.

Let L be the constant straight line distance between the contact points of the two fingers, θ_i the initial angle between the two fingers, θ the amount the part has rotated and y_i the initial displacement of the pre-loaded finger.

For the preloaded finger, the moment arm is given by

$$L_{pm}(\theta) = L\cos(\theta + \theta_i)$$

For the finger with the wedge, the moment arm is given by

$$L_{wm}(\theta) = L\sin(\theta + \theta_i)$$

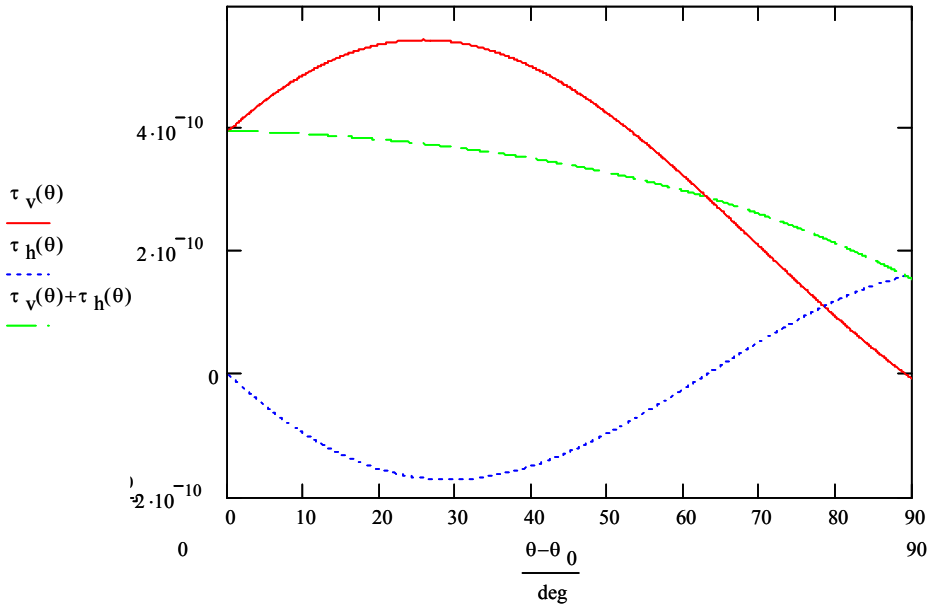

Figure 26: Torque exerted on connector during pick-up

Hence for each angle, the separation of the fingers is calculated and the force applied by each finger is determined based on the spring constants of the flexures on each finger. The force applied by the preloaded finger is given by

$$F_p(\theta) = k_p \times (y_i + L(\sin(\theta + \theta_i) - \sin(\theta_i)))$$

The force applied by the wedged finger is given by

$$F_w(\theta) = k_w \times L(\cos(\theta_i) - \cos(\theta_i + \theta))$$

The two torques oppose each other, with the wedged finger providing a counter clockwise torque and the preloaded finger providing a clockwise (positive) torque. They yield a net torque given by

$$\tau(\theta) = F_p(\theta)L_{pm}(\theta) - F_w(\theta)L_{wm}(\theta)$$
$$\tau(\theta) = \tau_v(\theta) + \tau_h(\theta)$$

The torque due to the two arms ($\tau_v(\theta)$ and $\tau_h(\theta)$) and the net torque ($\tau_v(\theta)+ \tau_h(\theta)$) are shown in Figure 26.

If the net torque is positive (clockwise) for all values of θ from 0 to 90^o, the orthogripper will work as envisioned. The orthogripper automatically stops at 90^o since at this point one of the fingers becomes parallel to a face of the rotating part and stops applying a torque on it.

The spring constant of the wedged finger is also important since it decides the final force with which a part is held after rotation. The force applied by this finger in the final state provides the normal force causing the friction which holds the part in place. Gravity is one of the forces which can cause the part to slip out. It is instructive to calculate the force due to gravity for a part of size 500μm x 500μm x 20μm

Considering silicon density of 2330 kg/m^3, this gives a weight of 1nN! Assuming a worst case coefficient of friction of 0.3 (as seen with a self assembled monolayer), the frictional force holding the part is given by $F_r = \mu \cdot k_w \cdot x$. In this design, k_w equals 1.62 N/m hence the frictional force F_r equals 4.8μN. This implies that the gripper will hold the part strongly even at accelerations up to 5000g.

Thus the more important constraint is to ensure that the part can be held strongly even while assembling the part into the socket. This necessitates that the insertion force into the socket be less than the force with which the part is held. In practice, it is found that the design problem is not over-constrained but in fact allows some range of possible

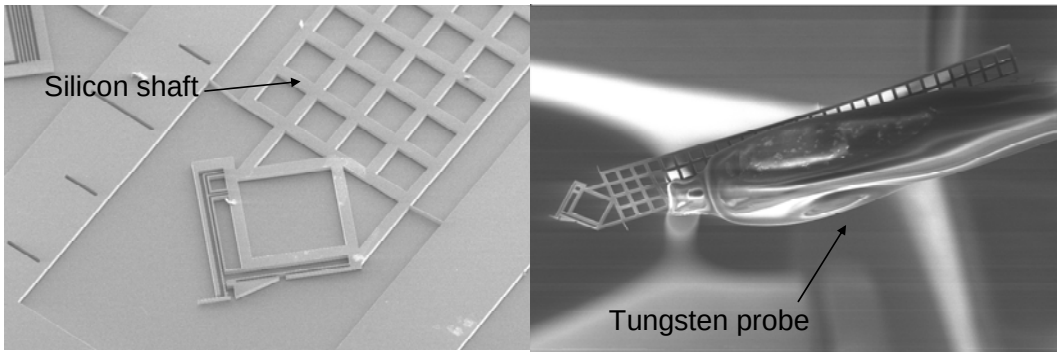

Figure 27: Attachment of orthogripper to tungsten probe

spring forces in the orthogripper etc. depending on application and desired final gripping strength.

3.3.2. Interfacing the orthogripper to the macro world

The tool used for pick and place microassembly in all cases mentioned above is a 3 to 6 degree of freedom micromanipulator to which the MEMS end-effector is attached. In our case, we accomplish this by fabricating the orthogripper at the end of a 5mm long silicon shaft (Figure 27). This shaft is used to provide a point of attachment to a tungsten probe which is mounted on a three DOF micromanipulator. A silicone adhesive called 'Amazing goop' is used to attach the shaft to the probe.

The shaft is attached to the probe as follows:

- A freshly fabricated chip is mounted on the chuck beneath the microscope
- The shaft is initially tethered to the device layer using 6 tethers
- A clean tungsten probe is used (Used probes work if cleaned with Iso-propyl-alcohol)
- Fresh silicone adhesive is dispensed to form a ~1cm size drop.

- The blunt end of the probe is inserted into the adhesive drop (while holding the other end with tweezers) such that about 3-4mm of it is coated with adhesive and then removed
- The adhesive forms a ~1mm layer coat on the probe
- The probe is then held over the chip and gently lowered onto the shaft while keeping the probe parallel to the surface of the chip
- When the epoxy comes into contact with the shaft, it is held there for 2-3 seconds then pulled upwards
- The bond between the epoxy and the shaft is strong enough to break the tethers holding the shaft in place
- The probe is then inserted into the three axis manipulator while ensuring that the shaft is perpendicular to the chip surface. In the current design, exact perpendicularity is not necessary.

The bonding of the shaft with the epoxy on the probe is not strong enough to break the tethers when the chip is coated with a self assembled monolayer [23] since this makes the chip hydrophobic. In this case, it is necessary to break the tethers with a micromanipulator mounted probe before trying attachment.

3.3.3. Testing results

This orthogripper has been extensively tested and performs well. However, a few problems were discovered during testing. Since the part is held by the two sidewalls in the final state nothing prevents the part from rotating perpendicular to this axis. This

results in the front of the part resting above (or below) the back. This problem can be corrected during the final assembly but results in further complicating the assembly.

The microparts are held in place by tethers which need to be broken by the gripper before the part is lifted up. It was discovered that designing tethers that break easily without moving the part in the grip of the orthogripper was a very challenging problem. Even if the tether was broken by a second probe tip, the resultant stress in the tether before it snapped sometimes caused the part to move or get dislodged from the gripper. Moreover, it was found that the rotation of the part depends to a large extent on the exact placement of the orthogripper with respect to the part. It is essential that the wedged finger slip into the oxide gap below the part for the orthogripper to work correctly. This is difficult to achieve in reality since it requires placement of orthogripper in the z-axis to within an accuracy of 1.5μm while observing the system with only a top view.

All of the above reasons indicate that automating this assembly process will prove to be difficult. Performing the assembly open loop will require some changes in the current process. One option is to have force/contact sensors on the fingers of the orthogripper to ensure that the part is properly held at all times. Another option is to use an actuated orthogripper where the two fingers are actuated using electrostatic/thermal actuators.

The orthogripper as currently designed is a useful tool for manual pick and place assembly of parts and can be used for production of small volumes of parts. Assembly yields close to 50% has been achieved during testing. The time taken for each assembly

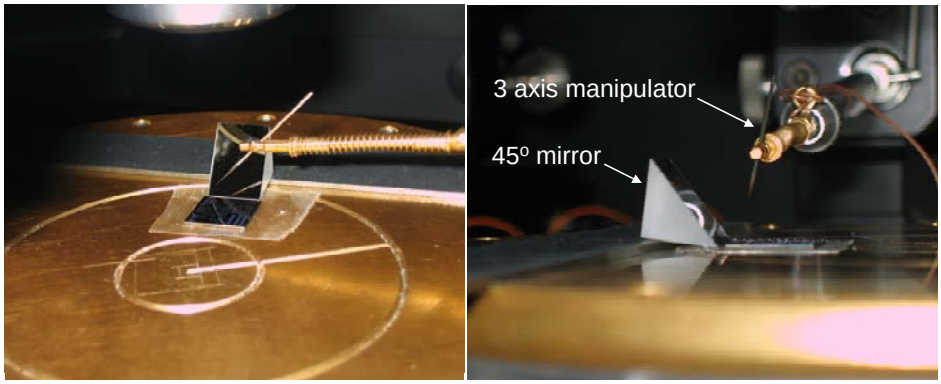

Figure 28: 45º mirror for perspective view during assembly

varies depending on the complexity of the part being assembled and can extend from 5-20 minutes. However, for large scale/automated assembly, the assembly process will have to be modified to make it more reliable and robust. One promising approach in this direction is presented in the next section.

3.4. Dual Chip Approach

One significant problem faced during assembly with the method described above is that only a top view is available while assembling the object. Since no information is available of the z-axis (except for knowing which parts are in the focal plane), it becomes difficult to know when you have lowered the gripper to the right height. One way to solve this problem is to integrate a second microscopic camera to the system which provides a perspective view. While this is possible, it adds to the clutter around the workspace and adds to the overall cost of the system.

One simple way to solve this problem is to place a 45º mirror next to the chip (Figure 28). This folds the path of light by 90º and presents the user with a side view of the chip. By tilting the mirror slightly, a stereoscopic view is obtained, significantly easing the task of

microassembly. This methodology has proved to be crucial in complicated assemblies to provide information about the position of parts in 3 dimensions. The 45^{o} mirror has been used to simplify assemblies using the orthogripper approach and also proves very useful for the dual chip approach.

All pick and place systems described so far use a device to pick up a part and rotate it by 90^{o}; either a robotic arm or a MEMS based rotation device. In either case, this rotation seems to be a cause of difficulty. The question then arises whether assembly can be achieved without the need for this 90^{o} rotation? The answer is yes! This is achieved by picking up microparts from one chip and assembling them onto sockets present on another chip which is oriented perpendicular to the first. So when a part is picked up from the first chip, it is automatically perpendicular to the plane of the second chip (Figure 29). This simple idea forms the basis of this approach and provides an elegant solution to the problem.

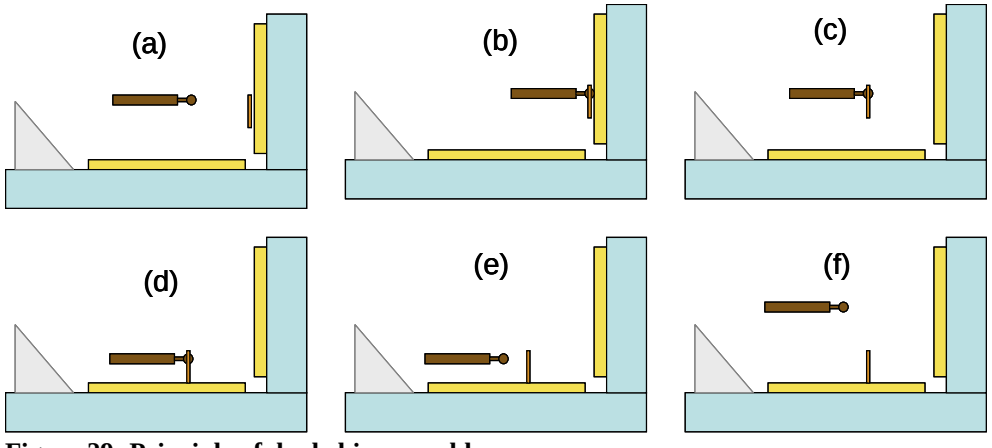

Figure 29: Principle of dual chip assembly

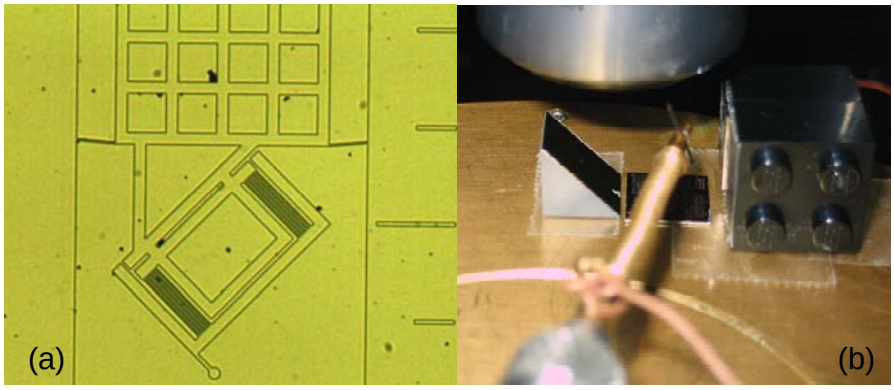

Figure 30: Setup for dual chip assembly. (a) Rigid end-effector (b) Setup on chuck

The only detail that needs to be taken care off is that the two chips are perpendicular to each other within a few degrees. The 45^{o} mirror can be used to get a view of the assembly on the side chip since it conveniently folds the path of light and provides a top view of the side chip. Thus we get a complete assembly system which sits on the chuck of the micromanipulator system (Figure 30b) and requires only the use of a three axis micromanipulator and a rigid end-effector.

A rigid end-effector (Figure 30a) was attached to a probe using a silicone adhesive as described earlier. This end-effector consists of a cylindrical tip which is used to grip the active connectors described in Section 3.4.1. One cause of concern in this approach is that the end-effector needs to be very close to perpendicular to one chip, else the wrong part of the end-effector comes into contact with the second chip during assembly. This can be achieved with careful mounting of the end-effector or by mounting it on a rectangular surface rather than a cylindrical tungsten probe.

3.4.1. Active connectors

Connectors which are picked up by the dual chip approach need an extra mechanism to grip the end-effector. The functional end of the end effector is designed to be a cylinder of radius 30μm. Hence a set of flexures placed 28μm away are used to interface with this end-effector (Figure 3a). During assembly, the end-effector is located above the flexures and lowered. The cylinder serves to pry open the flexures as it is lowered. In the opened state, the flexures exert a force on the cylinder thus ensuring that the part is held firmly. The force of this grip can be modified by changing the length of the flexures. For flexures of width b and length L, and final deflection 1μm, the spring constant (k) and grip force (F) are calculated as

$$b = 3\mu m$$
$$L = 170\mu m$$
$$\therefore k = \frac{3E \cdot I}{L^3} = 4.396\, {}^{N}\!/_{m}$$
$$\therefore F = k \cdot 1\mu m = 4.396\mu N$$

The connectors further have a flat surface which can be pushed against with the rigid end-effector to exert a force to aid assembly. The advantage of this approach is that the pickup of a connector using a rigid end effector is more robust than the pickup using two spring mounted fingers as in the case of the orthogripper.

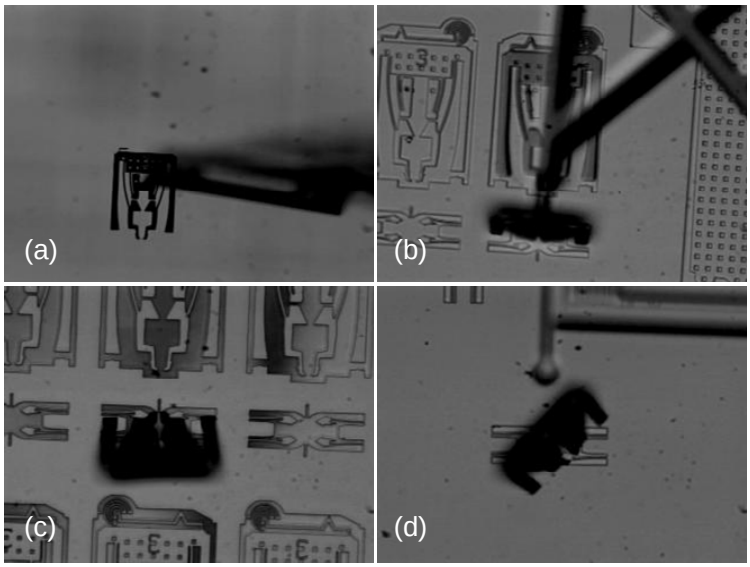

Figure 31: Assembly of Zyvex parts using dual-chip assembly techniques

3.4.2. Testing results

The Dual-chip approach of assembly was used to assemble two different kinds of connectors. One set were designs obtained from Zyvex [14] and fabricated in the Berkeley Microlab. These have a pickup location perpendicular to the final chip. This indicates that the flexures used to pick up the part are perpendicular to the surface of the chip when assembled. In this case, the end-effector can come in from the side, between the side-mounted chip and the mirror as shown in Figure 30b. Some devices assembled using this approach are shown in Figure 31.

The pick up and place proceeded perfectly but the final assembly was not perfect due to a design error in the parts. Figure 31a shows a connector being picked up from a chip placed on the chuck. Figure 31b shows the connector being placed on the chip mounted on the side as viewed through the 45^{o} mirror. Figure 31c shows the assembled structure while Figure 31d shows another attempt at assembly which was also partially successful.

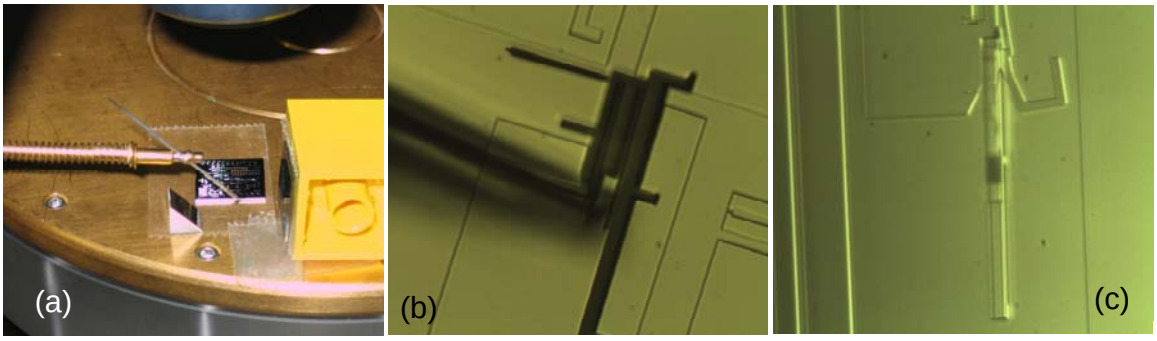

Figure 32: Dual chip assembly of our connectors. (a) Setup for assembly (b) Pick up of connector from bottom chip (c) Assembled connector on side chip as viewed through 45^{o} mirror

The other set of connectors assembled with this approach were our own connectors (described in Section 2.2). In this case, the pickup location is parallel to the final chip. This necessitates that the end-effector come in over the 45^{o} mirror and that we use a 5mm size mirror instead of a 10mm size mirror (Figure 32a). This approach worked as expected and a part was picked up and assembled as shown in Figure 32b and Figure 32c.

3.4.3. Pros and Cons

One advantage of pursuing this approach is that we have done away with the need for a rotation stage; which is in itself significant. Moreover, we have moved from a flimsy 2 fingered MEMS rotation stage to a robust end-effector. The advantages inherent in doing this are:

- The rigid end-effector has significantly higher stiffness and can deliver and tolerate much higher forces both in-plane and out-of-plane.
- The end-effector is itself capable of breaking the tethers holding the microparts in place as opposed to the orthogripper approach where a second probe is needed.

- By using a more robust, non-actuated end-effector the system's mean time to failure is increased, which is critical to high-throughput automated assembly

One disadvantage of this system is that the end-effector needs to be very close to perpendicular to the chip, otherwise the wrong part of the end-effector comes into contact with the second chip during assembly. Another issue is that the chips need to be mounted at a precise distance and orientation with respect to each other for the process to be automated.

Automation of this system can be achieved by adding visual feedback to the system. The assembly can still run 'open loop' as demonstrated in [14] and the visual feedback is used at the beginning of each assembly operation to orient the end-effector with a particular position on the die. A visual system satisfying these needs is presented in [24]. The visual system compares the optical image from the microscope to the chip layout provided in the form of a CIF file. The system measures translational, rotational and scaling differences between the two images. As a consequence, when the user selects a device to view on the CIF plot (or a device is selected automatically as part of an assembly sequence) the system moves the stage directly to the corresponding structure on the specimen stage. This work [24] was meant for testing of micromirrors but can easily be adapted for our application. This would provide a vision based feedback loop to help in correcting positional errors before automated assembly.

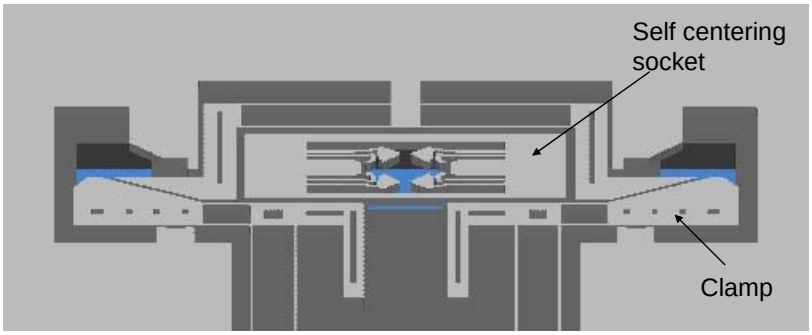

Figure 33: Zyvex sockets with clamps

Assembly of microparts designed for the Zyvex approach [14] and the orthogripper approach has been demonstrated using the dual chip approach. This has been achieved with a significant reduction in tooling and infrastructure required for the assembly. Hence this approach shows most promise for the design of an assembly-line style manufacturing station for production of complex micromechanical systems.

3.5. Self Centering Assembly

Vertical assembly (the connector is lowered vertically into a socket instead of horizontally along the plane as previously described) has been demonstrated in [14]. This requires the addition of a backside etch to make holes in the substrate below the socket to allow the connectors to be locked in the z-axis. While this significantly increases fabrication complexity, this approach leads to simpler automation since the only surfaces in contact are the connector and the socket (as opposed to connector sliding on substrate in horizontal assembly). This form of assembly was implemented with the connectors spring loaded in the final state to provide self centering.

The connectors are held in place by self centering sockets which can correct as much as 5μm of positional errors and still provide submicron accuracy in final assembly. This is

essential in applications like optical and electron columns where accuracy plays a very important role. One problem with this approach is that good electrical connectivity has not been demonstrated nor has a rigid mechanical connection. This is due to the self centering nature of the socket which necessitates the use of flexures and a weak contact force. An interesting way to solve this problem would be to assemble a part vertically into a self centering socket in a similar way as described. The connector would need an extra leg which would be placed in the L shaped opening of a clamp socket placed nearby. A similar design of a self centering socket with two clamps is shown in Figure 33. The connector for such a design would need two extra legs. In this case, the connector would get aligned to the sidewall of the clamp. If it is essential to preserve the self centering, it is possible to have the clamp socket suspended on parallel flexures instead.

After all the assemblies into self centering sockets are completed, a robust end effector could be used to engage all the clamps, thus ensuring that the part is clamped firmly in place. This combination of sockets ensures that each assembly stage needs only one end effector and gives the beneficial properties of both approaches.

Once we have figured out the design of microscale 'LEGO®' parts and the tools and techniques to assemble them we need to make assembled structures with interesting applications. Functionality can be added to the connectors in the form of actuators, compliant mechanisms, interfaces to in-plane actuators etc. Some applications of the assembled microstructures developed in our process are described in the next section.

4. Applications

What interesting devices can be designed given the ability to pick up microparts, rotate them by 90^{o}, and assemble them elsewhere with micron scale accuracy, such that they are held firmly at their final location? A few ideas are presented in this section.

4.1. Single Axis Rotation Stage

Assembling electrostatic actuators fabricated in a single mask SOI process is difficult due to the necessity of providing mechanical contact while maintaining electrical isolation between parts. However, it is possible with the addition of a nitride trench isolation step in the process [25]. In this step, trenches are etched in the device layer and then refilled with silicon nitride and undoped polysilicon leading to parts on the device layer which are mechanically connected but electrically isolated. Such parts could be picked up and assembled yielding very interesting vertical actuators like comb drives or even a vertical inchworm motor. This was not tried out due to the additional fabrication complexity involved.

Instead electrostatic actuators in the plane were interfaced to compliant mechanisms on assembled parts. Most assembled devices have the same 'front end' i.e. any of the connectors discussed in the previous section. Any functionality (in the form of movable parts) is added at the 'back end' of the device. This approach provides a library of connectors and sockets which can be added to different mechanisms to satisfy different applications. An interesting device based on this principle is a single axis rotation device. Such a device can be used as a mount for a reflecting surface, thus forming a single-axis

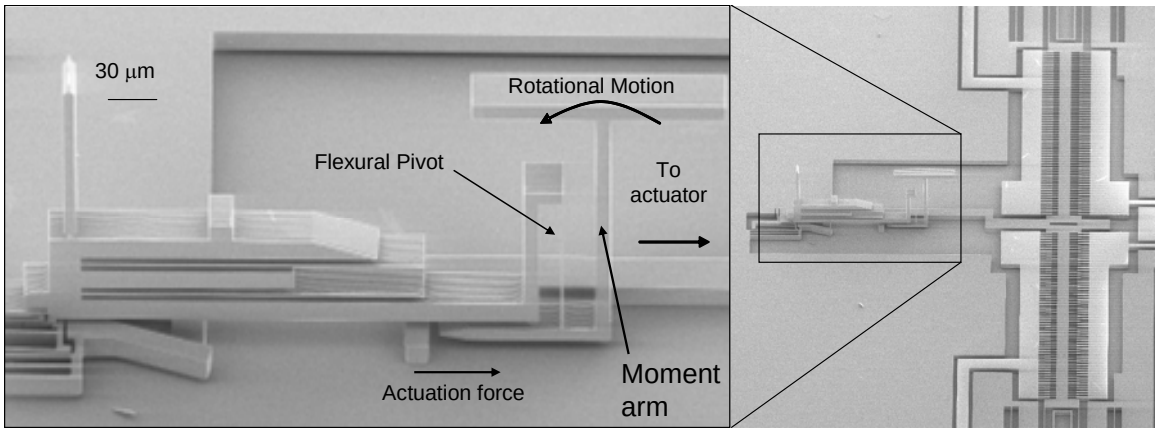

Figure 34: Single axis rotation stage (Principle of operation)

micromirror. It can also be used in any application where out-of-plane motion is desired like in the case of a robotic leg.

The front end of the rotation device consists of a connector described in Section 2 which is assembled into a rigid socket effectively anchoring the front. The back of the assembled part consists of a moment arm suspended by a flexure which forms the pivot (Figure 34). The mirror mount is located on top of the moment arm. The moment arm interfaces at the bottom to an in-plane actuator and converts the force applied by the actuator into a moment about the end of the flexure. Since the contact between the pivot arm and the actuator is friction based, slippage might occur at this interface during high frequency operation if the pivot is not preloaded. Different versions of this device were designed and tested: assembled into a snaplock or a clamp, versions with a straight or a serpentine flexure, different lengths of moment arm, and different interfaces to the in-plane actuator.

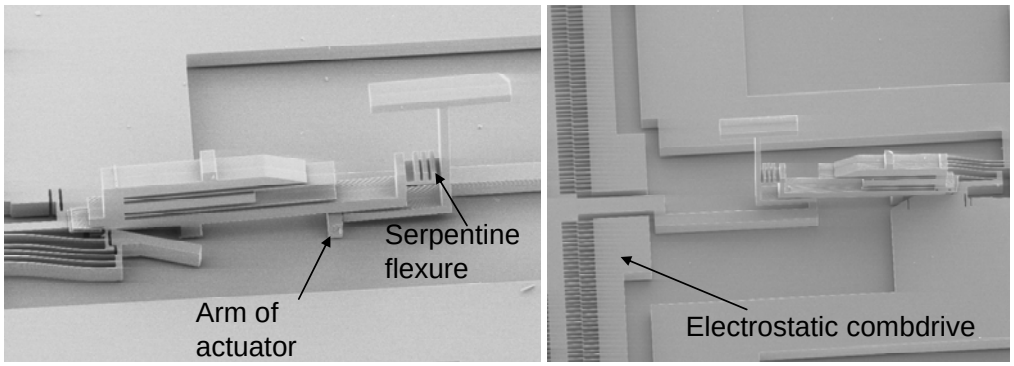

Figure 35: Single axis rotation stage with serpentine flexure

The largest deflection to date was obtained using the serpentine flexure shown in Figure 35 which showed 17^{o} of static mechanical rotation. Pull-in of the electrostatic actuators prevented higher angles from being achieved. We believe that significantly higher rotation angles can be achieved by adding minor design modifications. A different rotation stage (Figure 36) achieved 4.2^{o} of static mechanical rotation when a force of 7.9μN was applied using in-plane electrostatic actuators. The system was found to resonate at 3.75 kHz and attained a maximum rotation of 5.7^{o} at resonance.

Thus a single axis rotation stage is demonstrated which converts linear in-plane motion of an actuator to a rotational motion. A single axis micromirror can be created using this device by mounting a mirror face sheet as described in [18].

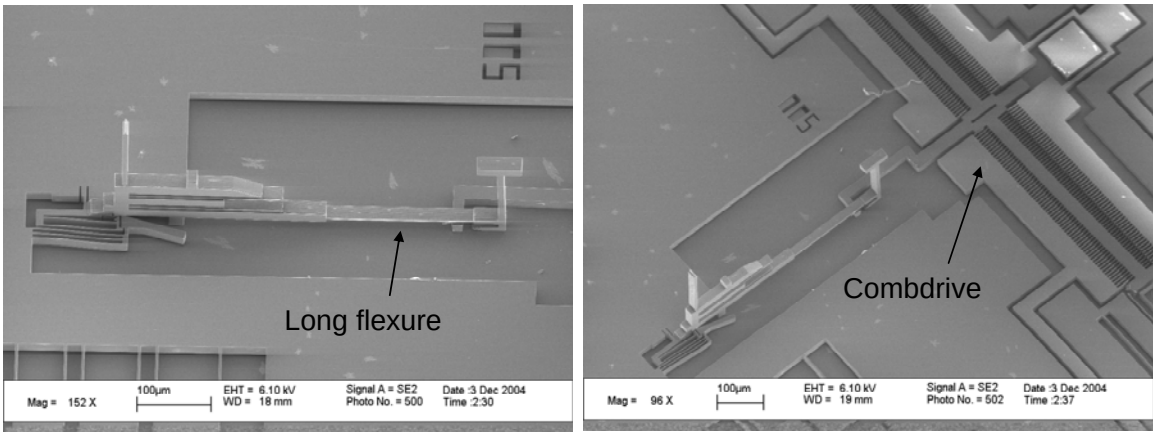

Figure 36: Single axis rotation stage with long flexure

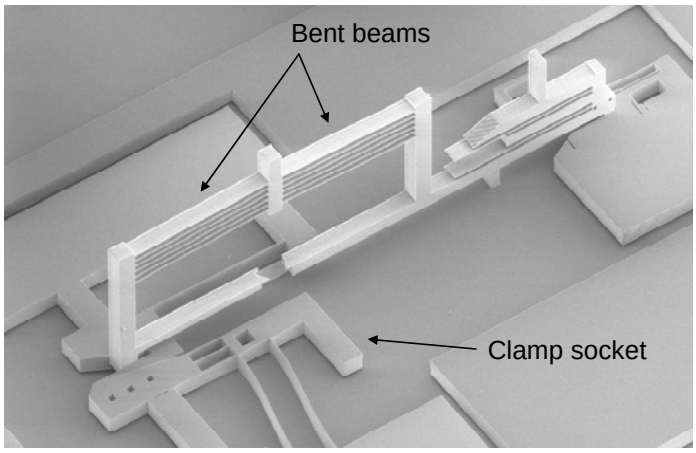

Figure 37: Vertical Bent beam Actuator

4.2. Vertical Bent-beam Thermal Actuator

Design of vertical actuators using MEMS is challenging in a single mask SOI process. As mentioned earlier, it is difficult to assemble electrostatic actuators to obtain vertical motion without the presence of a nitride isolation layer. However, it is possible to design thermal actuators which can be picked up and assembled since electrical isolation is not necessary.

A thermal bent beam actuator capable of large (>10μm) displacements and milliNewtons of force has been discussed in [26]. A similar bent beam thermal actuator was fabricated in plane, then picked up and assembled to provide vertical motion as shown in Figure 37. When a voltage is applied between the two legs of the device, a current flows through the thin beams (of length L) causing them to get hotter. This heating causes the beams to increase in length by ΔL. Since the beams are at a small angle ($\theta = 0.85^{o}$) to the horizontal, a small increase in length of the beams is gained up significantly to cause vertical deflection (ΔV). Assuming a coefficient of thermal expansion of α and a change in temperature of ΔT

$$\Delta L = L \cdot \alpha \cdot \Delta T$$

$$\Delta V = [L^2 + 2 \cdot L \cdot \Delta L - L^2 \cdot \cos^2(\theta)]^{1/2} - L \cdot \sin(\theta)$$

Thermal expansion leads to very small changes in length, so the total vertical displacement is only 2-4μm. However, this actuator is capable of generating large forces which might prove to be valuable in some applications. The angle θ cannot be reduced any further since a pre-bend angle in needed to ensure that the beams deflect in the desired direction. The actual force output was not measured due to the difficulty in setting up a measurement for measuring forces in the vertical direction.

The clamp socket plays a crucial role in the functioning of this device. First it provides a low resistance contact for the assembled part which is essential. Moreover, it provides a strong mechanical contact. If this were not the case, the beams would expand by changing the distance between the two assembled legs instead of raising the center in height. Preventing this motion is essential for the functioning of this device.

This actuator displayed lower displacements than expected. A similar structure fabricated in plane showed displacements larger by a factor of 2. The reason for this is not very clear but is thought to be the low thermal conductivity of the contacts of the assembled actuator compared to the one fabricated in-plane.

It is possible to gain up the displacement by using a lever mechanism and this was tried with some success. In this design, a part with three legs and two sets of bent beams was

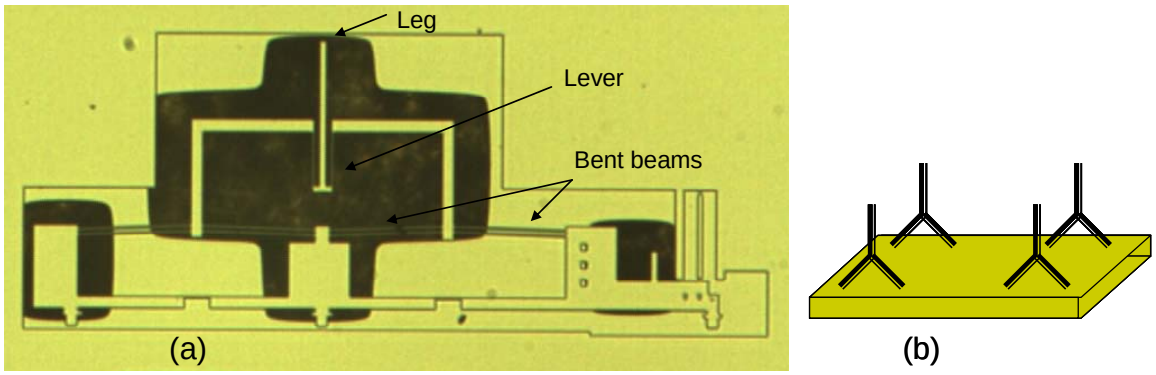

Figure 38: Leg for Microrobot (a) As fabricated (b) Concept of Microrobot

assembled into three sockets. The two thermal actuators were actuated independently and the lever was used to convert the differential motion to motion along an arc.

This motion can be used in the leg of a microrobot. A microrobot can be conceived off, which consists of a chip with four such assembled legs. The chip is then turned upside down and the robot can start walking due to the motion of these legs. By changing the length of the legs, force exerted by the actuator can be traded off for the displacement of the leg. In this particular design a gain of 2 was used. Motion of the leg was observed during testing but was again limited to less than 3µm. This can potentially be increased by increasing the length of the leg. However, a more fundamental problem seems to remain which causes the actuators to perform below expected levels. Another problem with this microrobot design is the use of thermal actuators which leads to high power consumption. Hence this design cannot be used for an autonomous robot.

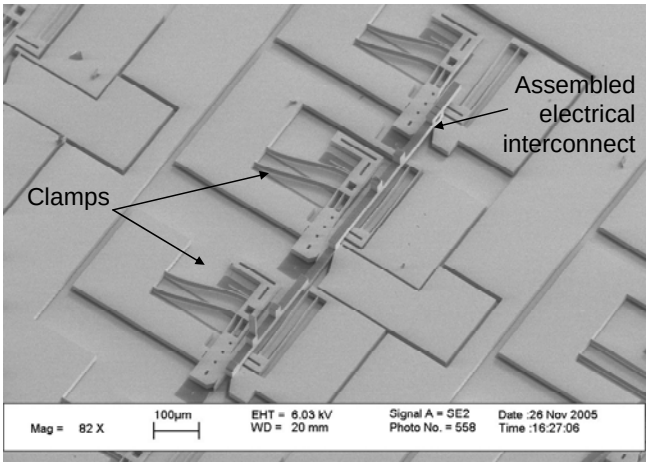

Figure 39: Multi-level electrical wiring using assembled parts

4.3. Multi-level Electrical Wiring

One of the major difficulties in using a single layer, single mask process is wiring to reach different sensors/actuators on the chip. If the actuation/sensing can be achieved with a single layer, it is unnecessary to use multiple structural layers for electrical connectivity. Instead, assembled parts as shown in Figure 39 can be used to achieve low resistance contacts between different parts on the chip. This could be particularly useful for complicated structures like bidirectional electrostatic inchworm motors which are very hard to wire up using a single layer. Assembled parts provide a cleaner solution than multiple wire bonds.

4.4. Structural Clips

Design of some actuators like rotary motors is severely constrained in a single layer process. Since the rotor cannot be constrained using flexures, it is impossible to prevent it from falling out when upturned. Such motors have traditionally been built using surface micromachined processes with multiple structural layers hence this was never an issue.

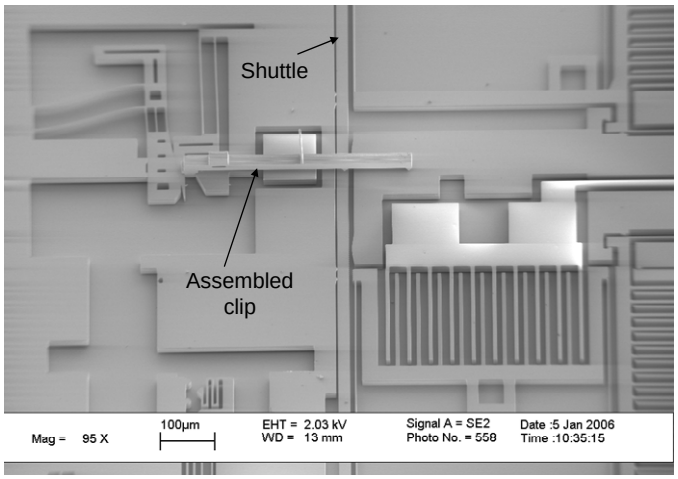

Figure 40: Assembled clip on inchworm shuttle acting as second structural layer

However, there are applications where an SOI process would be more suitable, hence the need for z-axis constraints.

This problem can be solved using a two layer SOI process in which two SOI wafers are independently processed, then flip-chip bonded as described in [27, 18]. Another option is to add polysilicon features on SOI wafers [17]. This requires a complicated process involving reflowing of glass to achieve planarization of the deep trenches before deposition of the polysilicon layers.

A simpler way to solve this problem is to assemble a clip on top of the rotor to act as a second structural layer. Test results shown in Section 3.4.1. indicate that parts assembled into clamp sockets can withstand more than 12mN of force in various direction. Hence the parts assembled into the socket can act as a strong structural layer.

This approach was used to constrain the shuttle of an inchworm motor as shown in Figure 40. This shuttle was designed to run on the substrate and hence was not attached by any flexures and is described in further detail in Section 5.5.

4.5. Stiction Test Structures

Stiction at the micro-scale is a poorly understood phenomenon. Even after the introduction of techniques like critical point drying, stiction often contributes to low yield of working devices and poor repeatability of experiments.

This problem was initially reduced by depositing a thin layer (30nm) of gold on the upper surface of the chips. This was primarily done to reduce the resistance of the parts but proved to have the interesting side effect of significantly reducing friction. Interestingly, coating the surface with a thicker layer of gold (300nm) seemed to worsen the coefficient of friction.

This phenomenon was later understood to be caused due to ploughing of asperities into the soft metal surface during sliding contact as explained in [28]. To achieve low friction, they suggest the use of a thin metallic film with low yield strength coated on a substrate with high hardness as was done in our case. They further suggest an optimum thickness of the metallic film to be used which matches with our results.

Another method used to reduce stiction was to make the surface highly hydrophobic to prevent interaction with water from the atmosphere. This was done by coating the surface

with a self assembled monolayer (SAM) which rendered the surface hydrophobic. This was done by using the AMST Molecular Vapor Deposition system to deposit a fluorinated organosilane monolayer (FDTS).

In either case, it would be interesting to calculate the change in the coefficient of friction of the surfaces before and after such treatment. Most previous studies of this nature have been performed by testing the coefficient of friction on sidewalls of devices. The primary cause of stiction in SOI structures is stiction of the device layer to the substrate. Since the sidewalls of an SOI process are significantly rougher than the atomically smooth surfaces of the oxide gap, this is likely to provide significantly different results.

To measure the coefficient of friction between the device layer and the substrate, a test structure is required to load the device layer against the substrate with a defined force and then push sideways with increasing force to observe when slippage begins to occur. Such a test structure is difficult if not impossible to design without vertical actuators.

An interesting alternative would be to test the coefficient of friction between two parts on the device layer which have been picked up and assembled onto arms of actuators. Two connectors can be designed with flat surfaces at their ends. They can then be picked up and one of them assembled into a fixed socket while the other one assembled into an X-Y actuator as shown in Figure 41. The two flat surfaces can then be brought into contact and a normal force applied on them using the Y actuator. The X actuator can then be used to apply a tangential force until slippage starts to occur. This would give the value of the

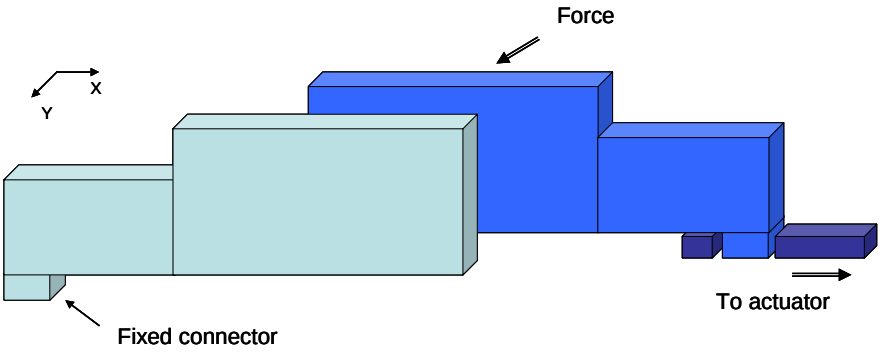

Figure 41: Coefficient of friction test structure

coefficient of friction. Since the atomically smooth surfaces of the two parts can be brought into contact, this should yield accurate values of the coefficient of friction.

4.6. Micro Bell-towers

To fulfill a long standing tradition among the MEMS assembly community at Berkeley, a micro-campanile was designed and assembled as shown in Figure 42.

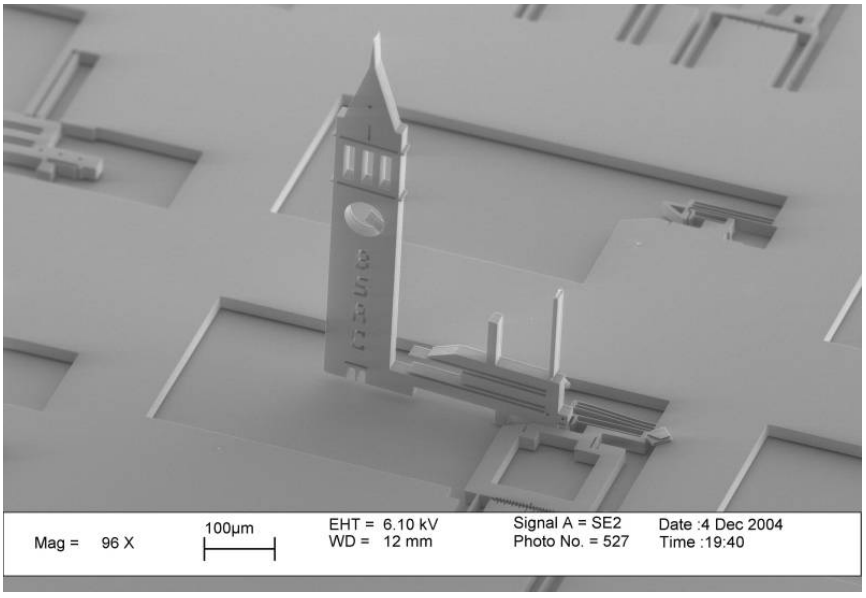

Figure 42: Berkeley Campanile

Pick and place microassembly can also be potentially used to build hybrid microsystems with components from non-compatible processes. This is particularly true in applications involving optics, sensors etc which tend to have non-compatible fabrications processes. However, it is possible that fluidic self assembly as demonstrated in [6] or flip chip bonding will provide a simpler solution in many of these applications.

Serial microassembly definitely provides an excellent technique to achieve complicated three dimensional structures capable of out-of-plane motion. It is also the technique of choice for precise assembly of complicated microparts as is required in applications like the electron lens for a mini-SEM. As ‘system on a chip’ applications begin to encompass various sensors and actuators on a single chip along with the integrated circuits, this technique could prove to be an essential manufacturing tool.

5. Silicon Spinneret

Microrobots as defined in {Dario, 1992 #33} are "a sort of 'modified chip' fabricated by means of silicon micromachining technologies, and containing micromotors, sensors and processing circuitry". Most microrobot work has concentrated on tethered walking microrobots as demonstrated in [30], [31]. However, microrobots become truly useful and deployable only when they are untethered, hence the push towards developing truly autonomous microrobots. An autonomous walking microrobot was demonstrated in [32] which operated off solar power. This microrobot experienced problems with its actuation mechanism which caused its motion to be closer to push-ups than to walking. An untethered microrobot has also been demonstrated in [33] but it requires that the surface it move on be powered. This requirement makes the actuation mechanism simpler to design but also significantly restricts the potential applications.

A major problem with walking microrobots is that they need to have either a very flat surface to walk on or large legs capable of complicated motions or a flexible body like a millipede. The first option limits the potential applications of such a system while the other two make fabrication of the robot on a single chip a difficult proposition. Potentially, the assembly techniques discussed in the previous sections could be used to assemble large legs capable of complicated motions, but that topic is left for another thesis. An interesting class of microrobots that hasn't been actively explored is microrobots that create the surface on which they move. This approach allows the design of the locomotion mechanism to be tailored specifically towards this surface.

Figure 43: Spider Spinneret. (a) Spider extruding a web from its spinneret (b) Electron microscope image of spinneret

This concept can further be extended to microrobots that build useful structures in which they later move around, much like a spider. This serves the dual purpose of letting the robot make complicated structures (scaffold for a large radio telescope in space) and then move around it performing tasks (fixing the parts broken due to meteorite hits). This section demonstrates preliminary work in developing the spinneret for such a silicon spider.

Spinnerets, as defined in the biological world, are organs located on the abdomens of spiders from which spider silk is extruded [34]. Individual spinnerets move independently yet in a highly coordinated manner to build cocoons or webs. An electron microscope image of a spinneret is shown in Figure 43.

In contrast, a silicon spider would have a spinneret made of a number of actuators which would be used to extrude a silicon ‘strut’. To create a silicon strut significantly larger than the spider, it is essential that the spinneret assemble small pieces together to create a much larger strut. This strut is then extruded out from the actuators and pieces added to it

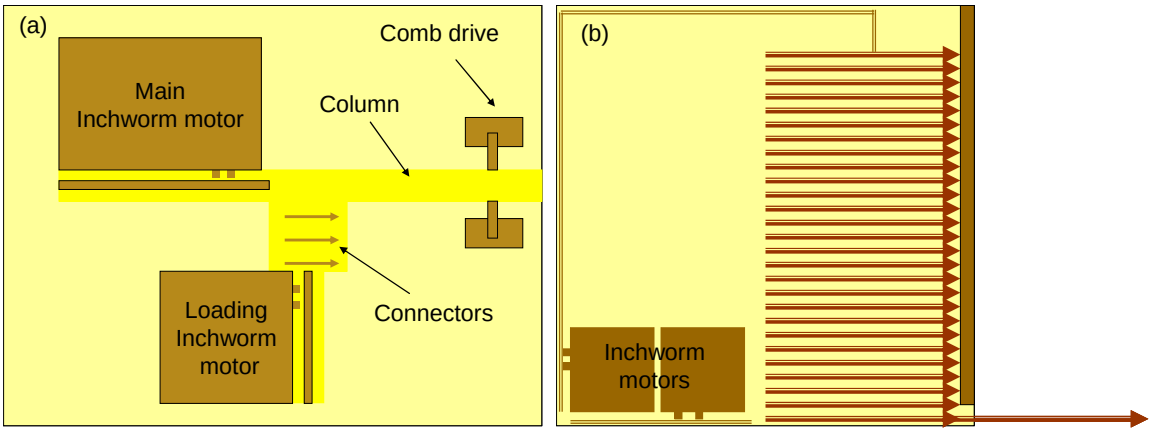

Figure 44: Silicon spinneret system. (a) System as envisioned in this work (b) Proposed system for spinneret of maximum length

at the base to extend its length. The pieces from which the strut is formed are referred to as connectors.

The actuators needed to assemble the silicon strut need to have a large range of motion (100s of μm) as well as be capable of generating large forces (100s of μN). Since the final robot is expected to be autonomous, it is also essential that the actuators consume low power. Electrostatic inchworm motors demonstrated in [35] satisfy most of these requirements and are used as the actuators in these spinnerets.

5.1. System Operation

The spinneret is envisioned as shown in Figure 44a. Connectors would initially be stacked in a chamber and connected to the device layer by tethers. The loading inchworm motor and the main inchworm would be used to push the connectors into the column and to assemble them into a strut. Comb drives at the end of the column would be used to hold the connectors in place during assembly. All of the components described above can be fabricated in the single mask SOI process described in [18].

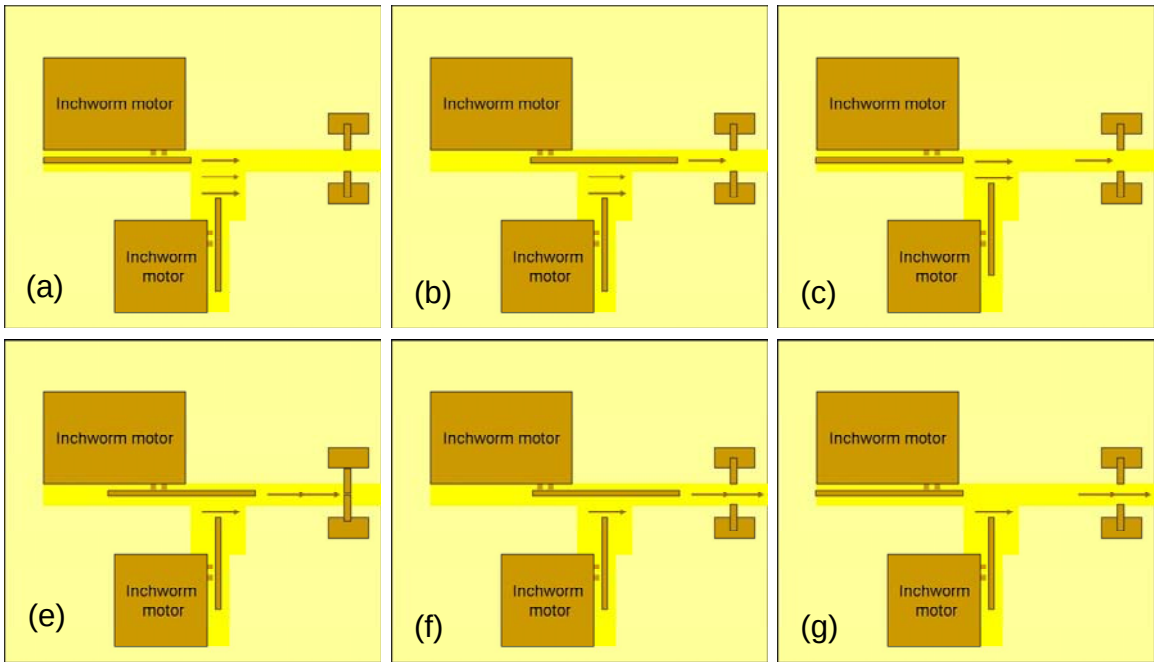

Figure 45: Principle of operation of spinneret

The principle of operation of the spinneret is shown in Figure 45.

a) After breaking the tethers, the connectors are pushed into the column using the loading inchworm motor.

b) After the first connector enters the column, the main inchworm motor pushes the connector along the column until enough space is created for the next connector to be introduced into the column.

c) The main inchworm motor then retreats and a second connector is introduced into the column by the loading inchworm.

d) This connector is then pushed by the main inchworm until the first connector is stopped by the actuated comb drives. These comb drives provide the restraining force to hold the first connector while the second one is added to the strut.

e) The comb drives then retreat to open the column and the connectors are pushed out by a connector length.

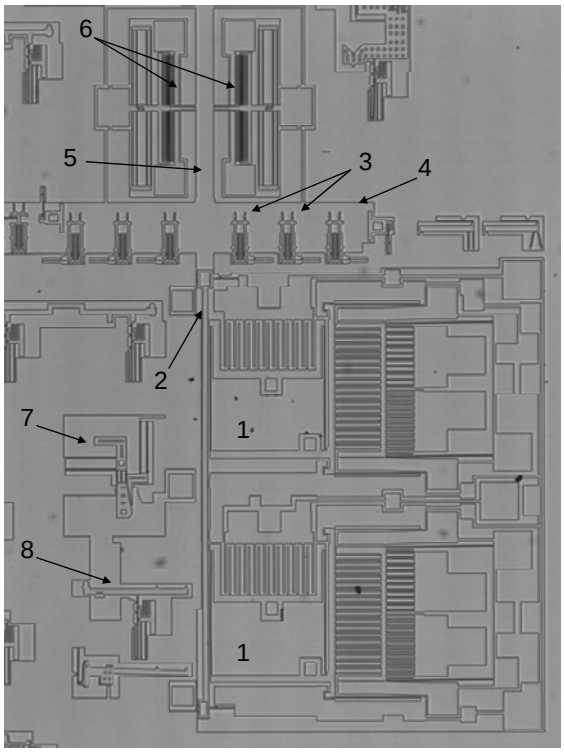

Figure 46: Micrograph of fabricated spinneret consists of (1) Bidirectional inchworm motor(2) Shuttle of inchworm (3) Connectors which form 'strut' (4) Chamber in which connectors are fabricated (5) Channel in which they get assembled using the inchworm (6) Comb drives which help to restrain connectors (7) Socket for assembling clip on shuttle (8) Clip which gets assembled

f) This then provides enough space for the introduction of another connector into the column from the chamber and the process repeats. Thus a silicon strut is formed and extruded out by the spinneret.

It is interesting to calculate the length of the longest strut that can be extruded from a $1cm^2$ chip. This number is arrived at by considering the system shown in Figure 44b. A main inchworm and a loading inchworm of size 2mm*2mm are assumed. Each connector is assumed 6mm long and 100µm wide. 90 of them can be stacked side by side in a chip of width 1cm, with a 90% fill factor. This gives a strut of length 90*6mm = 540mm = 0.5m!

The actual system as fabricated is shown in Figure 46. To demonstrate the proof of concept, no loading inchworm motor is present and the loading of connectors into the

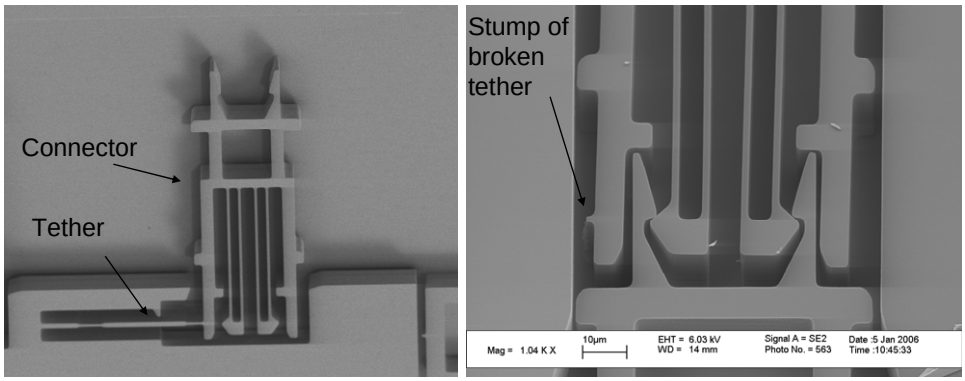

Figure 47: Tether design for connector

channel is instead performed with micro-manipulator operated probe tips. Ideally the tether breaking would also be automated but this technique hasn't been developed yet. Instead the tethers are broken using probe tips to setup the system.

5.2. Tether Design

The design of tethers which hold the connectors in place is particularly difficult since they need to meet a number of specifications. When broken with the probe tip, it is important that the connectors are not turned into projectiles and that the tether pieces do not create debris in the area. Further, it is important that the tether breaks very close to the base so that the stumps left on the connector and on the device layer do not interfere with the assembly operations.

A number of tether designs were experimented with to achieve these goals. The final design is shown in Figure 47. Testing shows that the tether breaks less than 2µm from the connector and the stump left attached to the device layer does not obstruct the chamber due to its position.

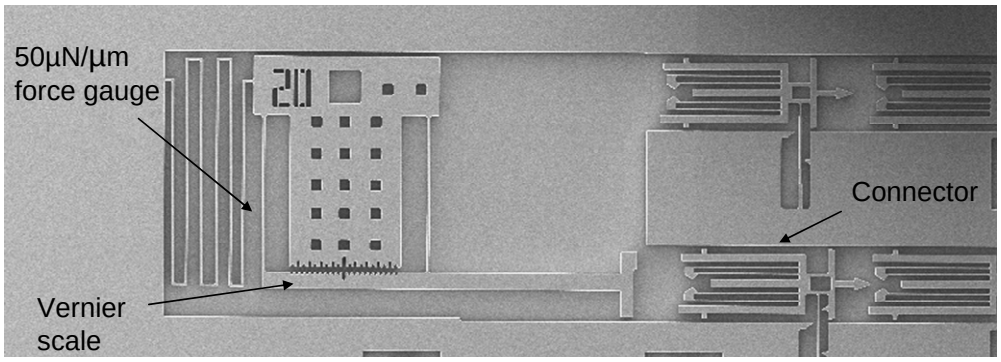

Figure 48: Force test for testing insertion force of connectors and frictional force

5.3. Stiction

Once the tethers are broken, the connectors fall on the substrate of the chip. For the system to function as envisioned, it is essential that the connectors not experience stiction with the substrate. If no special care is taken, it is found that the connectors get firmly stuck to the substrate as soon as they come in contact since the two surfaces in contact are atomically smooth.

As mentioned in Section 4.5, a self assembled monolayer (SAM) of a fluorinated organosilane is added to the surface soon after the release. This passivates the silicon surfaces and makes them highly hydrophobic. This procedure is seen to reduce stiction to a large extent and was found to be essential for the connectors to work properly. Force tests were performed using the device shown in Figure 48 to investigate the force needed to push a connector lying on the substrate. These tests yielded values as low as 25µN. However, it was sometimes seen that the parts were completely stuck even in the presence of the SAM coating. The SAM coating seems effective in reducing the probability of two surfaces to come in close contact but seems ineffective in preventing stiction once such close contact occurs.

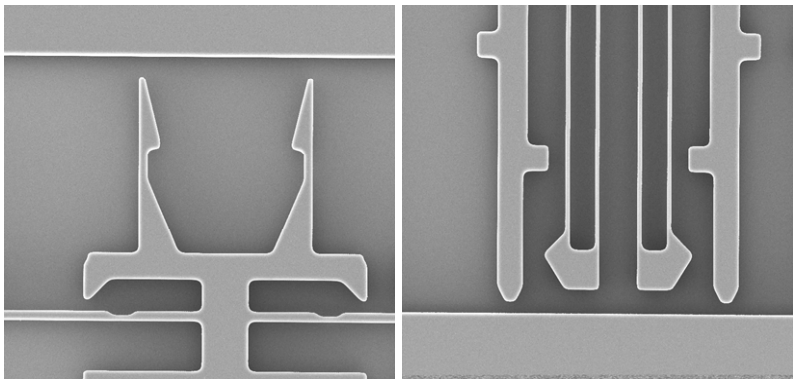

Figure 49: Connector design

5.4. Connectors

The connectors need to be designed such that they can be pushed sideways out of the chamber and along the channel without rotating. Since the entire assembly operation is designed to be automated, it is essential that the parts self center during assembly. Hence all the edges on the connectors and the channel along which they move are chamfered. As discussed in Section 2, all the chamfered surfaces are at an angle of greater than 71.5^{o}. The assembling parts are designed based on the snap locks described in Section 2.

To simplify assembly and create a strong strut, the connectors are designed to have a low insertion force and a high pullout force. The insertion force of the connectors is designed to be less than 100μN since the maximum force exerted by the inchworm motors is 200μN. The front and back end of the connectors are shown in Figure 49.

The forces required for assembly are calculated as follows

$h := 20um$ height of beam

$b := 2um$ width of beam

$I := \frac{b^3 \cdot h}{12}$ $I = 1.333 \times 10^{-23}\ m^4$

$E := 160 \cdot 10^9 Pa$

$l := 50um$ this defines half the length of the beam

$k := 3 \cdot E \cdot \frac{I}{l^3}$

$k = 51.2 \frac{N}{m}$ defines k of 2 parallel bars of length 100

$open := 3.4um$ Distance the flexures need to open to assemble

$tan := \frac{2.5}{10}$ The slope of the head which leads to a reduction in required force

$F_{open} := 2k \cdot open \cdot tan$

$F_{open} = 8.704 \times 10^{-5} N$

In this calculation, the overetch of parts is ignored, which leads to a reduction in required force. However, some extra force is required to overcome the force of stiction. The force with which two connectors grip each other is calculated to be

$grip := 2.2um$

$F_{grip} := 2k \cdot grip$

$F_{grip} = 2.253 \times 10^{-4} N$

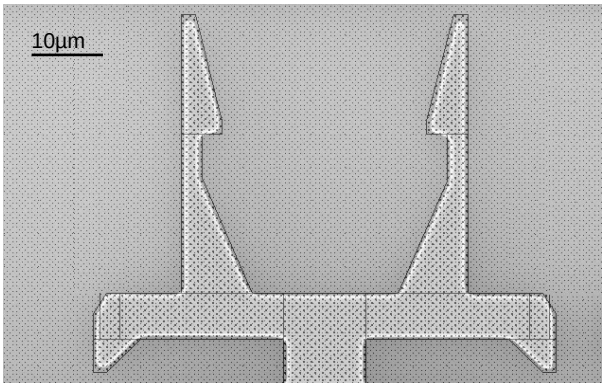

Figure 50: Comparison of layout and actual fabricated structures

The force required to pull a connector out in the opposite direction to which it was assembled is significantly higher than the force required to assemble two connectors due to the difference in angle of surfaces in contact

$$F_{escape} := 2k \cdot open \cdot 1$$

$$F_{escape} = 3.482 \times 10^{-4}\ N$$

The force taken to assemble these connectors is verified using force gauges and found to be between 100-150µN. The setup used to take force measurements is shown in Figure 48. However, the exact force taken to assemble two connectors is a strong function of the over-etch present in a particular run. The over etch of beams changes the thickness of the flexures and the spring constant depends on the third power of the thickness. Moreover, the rounding of the corners decides the distance that the flexures actually need to deform for assembly. A comparison of the layout of the connectors and the actual fabricated shape is shown in Figure 50. This comparison helps to better calculate the actual values of insertion force, pullout force, and force with which the parts are held together taking into account fabrication non-idealities. The force to push a connector against the

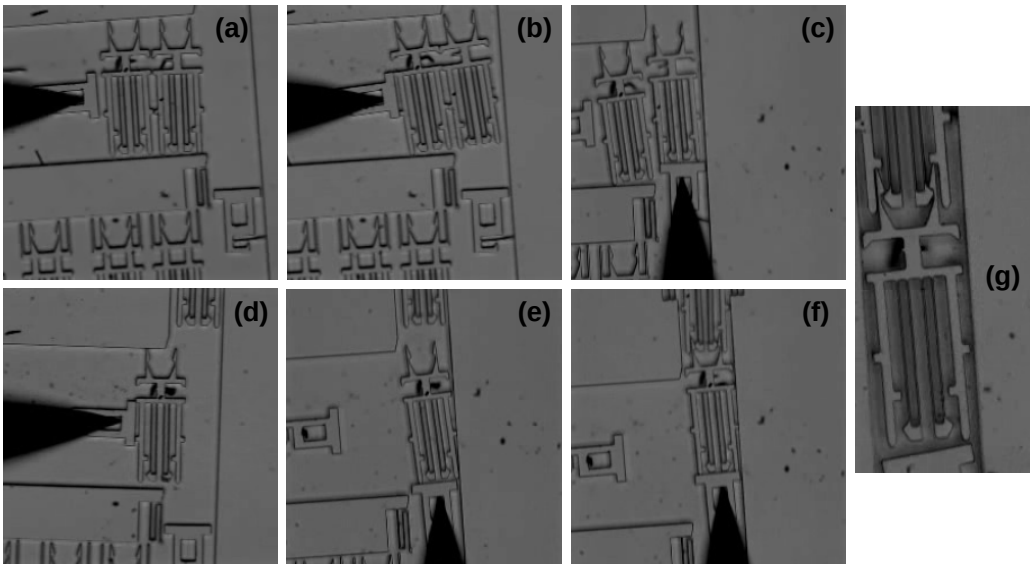

Figure 51: Testing of connectors

frictional force with the substrate adds to the force required for assembly. Thus the actual force required to perform assembly is difficult to calculate analytically.

The system was first tested using micromanipulator mounted probe tips instead of inchworm motors. Video captures from this round of testing are shown in Figure 51. It was realized at this stage that the clearance between the sidewalls and the connectors needs to be as low as 1μm for the system to function. Larger clearances allow the part to rotate during assembly, which can lead to errors. One option in this regard (which was not tried) is to use sidewalls of the channel held in place by flexures such that the distance between them is less than the width of the connectors. This ensures that the connectors are always exactly self-centered, but increases the frictional force on their sides.

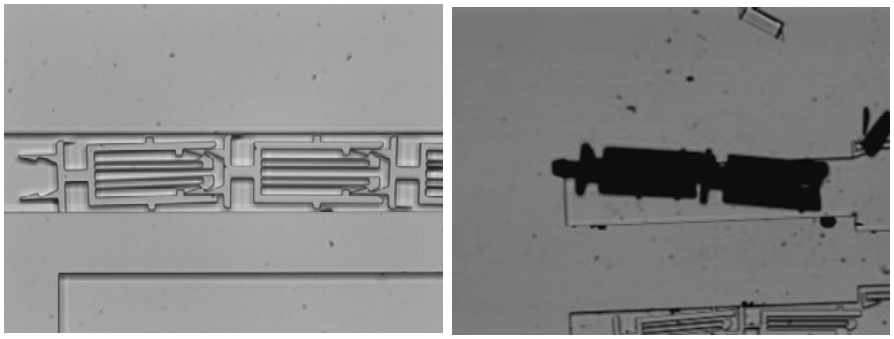

Figure 52: Strut of connectors

Up to four connectors have been successfully connected to form a strut. These connectors stay assembled even when picked up out of plane (Figure 52) indicating that they are held in place by frictional forces as expected.

5.5. Inchworm motors

Electrostatic gap closing inchworm motors presented in [35] decouple actuator force from total travel and allows the use of electrostatic gap-closing actuators to achieve large force and large displacement while consuming low power. The basic design of inchworm motors is presented in [35].

Electrostatic inchworm motors traditionally use parallel-bar flexures to suspend the moving shuttle. These flexures limit the maximum displacement of the motor and also reduce the net force exerted by the motor. A shuttle not constrained by flexures was demonstrated in [36]. One problem with a free shuttle is that it isn't constrained in the z-axis. This problem was solved in [36] by using flaps to constrain the out-of-plane motion of the shuttle. This required a complex five mask fabrication process that combined two polysilicon structural layers with thick SOI structures and a backside etch.

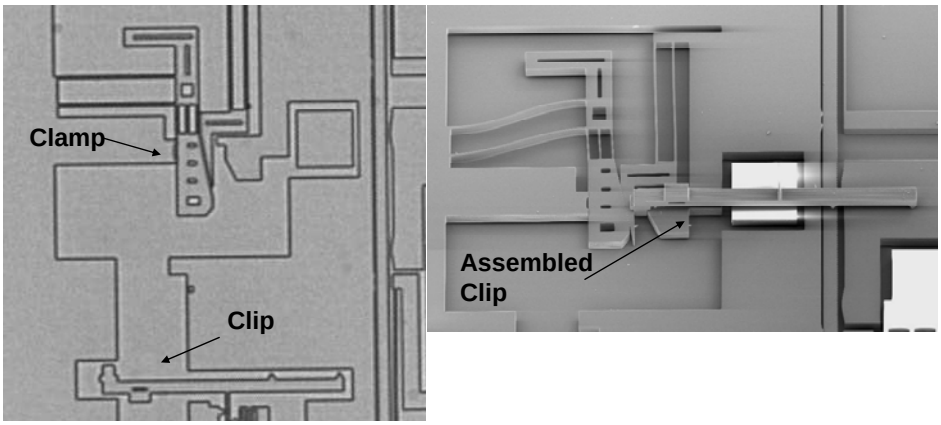

Figure 53: Assembled clamp on untethered shuttle of inchworm motor

The ability to 'pick and place' assemble parts into mechanically rigid sockets as demonstrated in the previous sections allows us to use a single mask SOI process and assemble clips that constrain the out-of-plane motion of untethered parts. This arrangement is shown in Figure 53 where a clip has been assembled into a clamp connector to constrain the shuttle. Another problem with this approach is that the shuttle now runs on the substrate and therefore experiences strong stiction. This is reduced to a large extent using the SAM coating described in Section 4.5.

Since the shuttle needs to be free standing during operation, it also needs to be initially tethered like the connectors. This tether faces similar constraints as the tether on the connectors in that it is essential that the tether break cleanly and close to the point of attachment. This is achieved with a similar tether design to that presented in Section 5.2 and is shown in Figure 54.

A bidirectional inchworm motor was designed and fabricated and is shown in Figure 46. It uses biasing electrodes to bias the drive electrode which decides the direction of motion of the shuttle. A bidirectional actuator is needed when the shuttle runs untethered on the

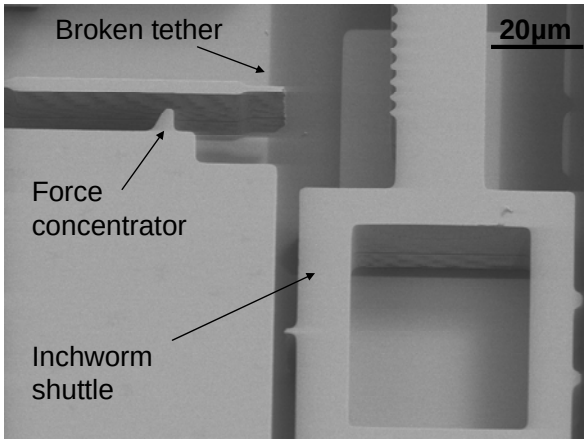

Figure 54: Broken tether on shuttle of inchworm motor

substrate since flexures are no longer present to bring back the shuttle to its initial position. For a gap closer array with 'n' fingers of length 'L' and height 'h' each, spacing between fingers being d and d_2 alternately and a voltage 'v' applied between the two electrodes, the initial force 'F' applied by the actuator is calculated as

$$F := \frac{1}{2}\frac{n\cdot\varepsilon\cdot h\cdot v^2\cdot L}{d^2} - \frac{1}{2}\frac{n\cdot\varepsilon\cdot h\cdot v^2\cdot L}{d_2^{\,2}}$$

This equation is used to calculate the force exerted by the gap closer arrays of the inchworm motor at the initial gap width. The initial gap width is used in the equations since it defines the maximum load that can be supported by the actuator. The fabricated drive electrode was capable of supporting a load of 208µN at 160V. The clutch was run at 50V which corresponds to a force of 43µN. The current design has been tested to move more than 330µm. The only fundamental limit on how far the actuator can move is the length of the shuttle which is around 1mm in this case.

Figure 55 shows a connector being pushed by the shuttle. The shuttle was seen to push the connector in jerks as is expected due to the stepping nature of the inchworm motion.

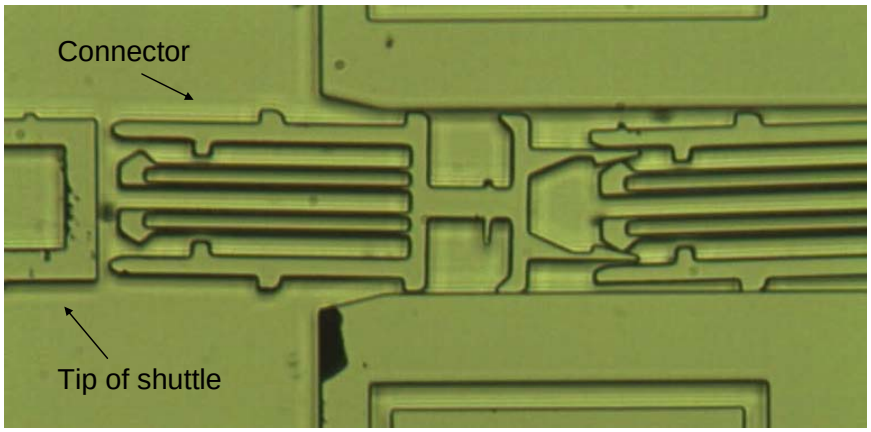

Figure 55: Inchworm motor assembling a connector

The self-centering mechanisms worked as expected, and the connectors were seen to recover from positional errors as high as 15^{o}. When two connectors were brought into contact for an assembly, it was seen that the force produced by the inchworm was insufficient to open the flexures on the connector and allow assembly to take place. Hence the connectors did not actually click into place. This was probably due to larger stiction forces than anticipated. Another cause of the problem could be a lower overetch than expected, thus increasing the spring constants on the beams on the connectors. However, this problem can be easily resolved by designing inchworm motors capable of a higher force output or connectors with weaker flexures.

Thus assembly of connectors to form a 'silicon strut' using an inchworm motor with extended range is demonstrated. This work forms the first step towards the realization of a spiderbot. A few ideas for future work in this direction are presented in the next subsection.

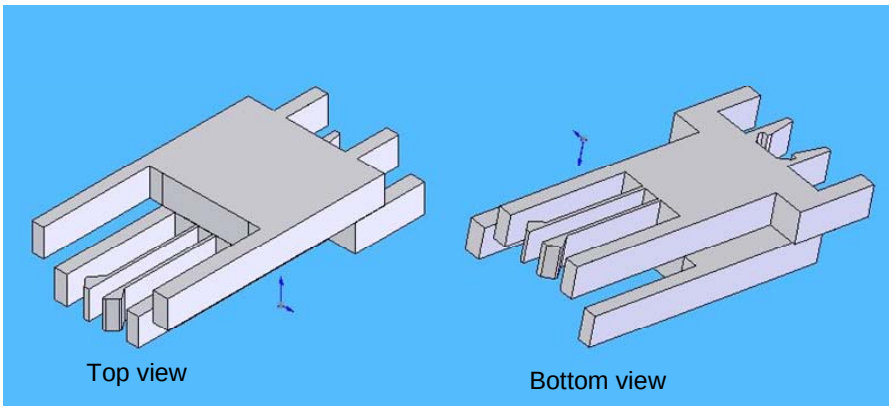

Figure 56: Modified connector for robust strut

5.6. The Spiderbot

A few designs for connectors, motors and locomotion are presented here which could help make the world's first silicon spider.

5.6.1. Multi-layer Connectors

One major drawback with the current connectors is the lack of constraints along the z-axis. The only constraint along the z-axis is the frictional force of the flexures holding the connectors together. To make a robust strut with snapped together connectors, it is important to use a multi-layer process. Either a polysilicon process like PolyMUMPs can be used or a two layer SOI process like described in [37] can be used. A design of a connector made using a 2 layer process is shown in Figure 56. It uses the same basic principle as the connectors discussed in this thesis but uses the additional structural layers to provide interlocking 3D mechanisms. Either a gap material between the two layers or an extra uniform etch of all exposed surfaces at the end is necessary to ensure some clearance between surfaces.

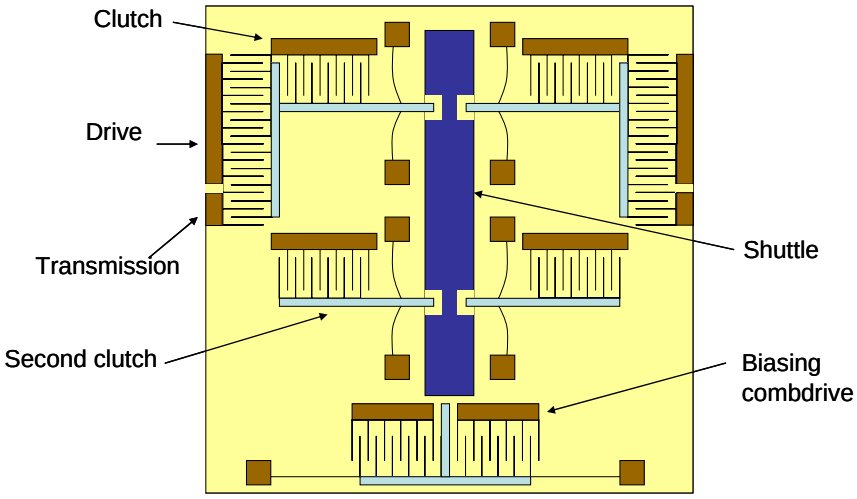

Figure 57: Transmission based inchworm motor

5.6.2. Transmission-based Inchworm Motors

One possible modification of the inchworm motor is the addition of a transmission to the drive of the inchworm. The transmission serves to reduce the initial gap between the gap closers on the drive actuator which leads to an increase in the drive force. Using a transmission reduces the step size (and hence speed) but that isn't a major concern in this application. The reduction of the step size also necessitates the use of clutches with no teeth since the pitch of the teeth is limited by the minimum line and space of the fabrication process. Two clutches can be used to grip the shuttle from both sides.

If the two clutches are designed using gap closing actuators, the force exerted by the actuators increases as the gap width decreases. Hence the equilibrium point at the center is an unstable equilibrium point and the clutches tend to operate such that one of the clutches overpowers the other to close completely. This leads to either shorting of the clutches or the shuttle touching a gap-stop.

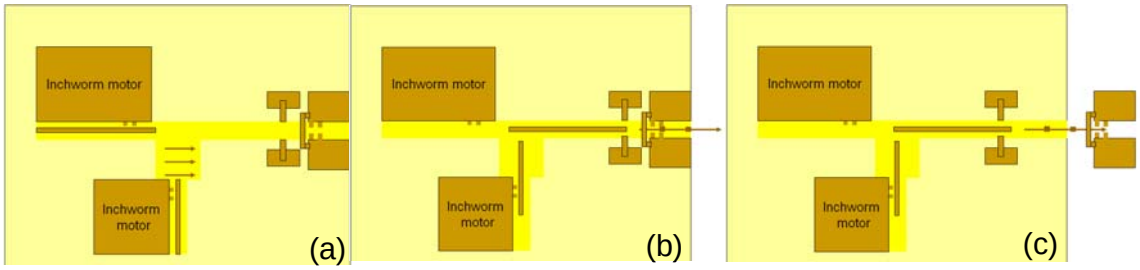

Figure 58: The Spiderbot

A better design uses a gap closing actuator to open the clutch and uses the spring forces on the suspension to close the clutch. Since the spring force decreases as the gap width decreases, this acts as a stable equilibrium point. One constraint with this approach is that the shuttle should be held tightly in the un-actuated state of the clutch. It is impossible to fabricate a shuttle in this state since the beams on the clutch would need to be pre-stressed. This problem can be solved by using the structure shown in Figure 57 which has gaps in the shuttle where the clutches initially rest. The clutches are first opened using the gap-closers, following which the shuttle is pushed forward using a biasing comb drive at the base. When the clutches are now released they grip the shuttle with no applied voltage. An extra pair of clutches is used to keep the shuttle in place during the half cycle when the drive-clutches are not engaged.

5.6.3. System Design

A silicon spider could use an inchworm motor to hang from the strut and climb along it using the same motion as used to push the shuttle in a conventional inchworm. The connectors can have teeth on the side to help the inchworm's clutching mechanism. Else, an inchworm with no teeth but a stronger clutch to deliver sufficient drive force can be used.

A simple spider robot can be visualized as shown in Figure 58. It consists of the spinneret and a small breakaway robot. The breakaway robot uses an inchworm motor to move along the strut by grasping at its sides. Advantages of using a breakaway robot are the reduction of size and weight of the mobile system and the design of its inchworm to exactly meet the specifications required for motion. A more advanced design would have the entire chip along with the spinneret move along the strut. The advantage of reusing the system is possible reuse of one of the inchworm motors of the spinneret for locomotion. Moreover, this gives the robot the ability to move along the strut and add structures at different locations.

This section presents preliminary work on development of a silicon spinneret. Initial designs and testing results are presented which show that an inchworm motor can be used to assemble connectors and extrude a silicon strut. A few ideas for the development of a complete silicon spider which can extrude a strut and then climb along it are also presented. Such a silicon spider would be an important addition to the small world of microrobots and presents an interesting area for future research.

6. Conclusion

Monolithic fabrication, hinged assembly and self assembly using stochastic processes are all examples of techniques which have been used for MEMS fabrication. While an impressive array of devices have been fabricated using these techniques, complicated three dimensional microstructures require the use of complicated fabrication processes with low yield. This thesis demonstrates that serial assembly can be used successfully to manufacture some impressive three dimensional microstructures using parts manufactured in a simple single-layer process.

Two assembly approaches, design of microparts for assembly and the tooling required for pick and place assembly are presented. The demonstration of automated assembly of connectors in the spinneret indicates that serial assembly can be automated with careful design. I believe that miniaturization of systems and the requirements for packaging of hybrid systems made from components from mutually incompatible processes will make pick and place microassembly a widely used manufacturing technique in the future. While the 'killer applications' for this technique have not yet been discovered, the increasing interest from academia and industry provides hope.

It is hoped that the information included in this thesis will provide the platform for others to develop similar assembly techniques. The design decisions and their pros and cons discussed in the thesis should provide a good starting point. An interesting direction for future research would be to integrate visual feedback and stepper motors to this work to

create an automated assembly technique for manufacture of complicated hybrid microsystems.

References

1. R.S.Fearing. *Survey of Sticking effects for Micro-parts*. in *IEEE Int. Conf. Robotics and Intelligent Systems IROS '95*. 1995. Pittsburgh, PA.
2. Cohn M.B., et al. *Microassembly Technologies for MEMS*. in *SPIE Micromachining and Microfabrication, Conference on Micromachining and Microfabrication Process Technology IV*. 1998. Santa Clara, Ca.
3. Singh A., et al. *Batch Transfer of Microstructures using flip-chip solder bump bonding*. in *Transducers 97*. 1997. Chicago.
4. Srinivasan U., D. Liepmann, and R.T. Howe, *Microstructure to Substrate Self-Assembly Using Capillary Forces.* Journal of Microelectromechanical Systems, 2001. 10(1): p. 17-25.
5. Cohn M.B., C.J. Kim, and A.P. Pisano. *Self-Assembling Electrical Networks: An Application of Micromachining Technology*. in *Transducers '91 International Conference on Solid-State Sensors and Actuators*. 1991. San Francisco.
6. *FSA Manufacturing* http://www.alientechnology.com/technology/fsa_manufacturing.php.
7. Srinivasan U., et al., *Fluidic self-assembly of micromirrors onto microactuators using capillary forces.* IEEE Journal of Selected topics in Quantum Electronics, 2002. 8(1): p. 4-11.
8. Pister K.S.J. *Hinged polysilicon structures with integrated CMOS TFTs*. in *Solid-State Sensor and Actuator Workshop, 1992*. 1992.
9. Fukuta Y., et al. *Microactuated self-assembling of 3D polysilicon structures with reshaping technology*. in *Tenth Annual International Workshop on Micro Electro Mechanical Systems, 1997. MEMS '97,*. 1997.
10. Green P.W., R.R.A. Syms, and E.M. Yeatman, *Demonstration of three-dimensional microstructure self-assembly.* Journal of Microelectromechanical Systems, 1995. 4(4): p. 170 - 176.
11. Guckel H., T. Christenson, and K. Skrobis, *Metal micromechanisms via deep x-ray Iithography, electroplating and assembly.* Journal of Micromechanics and Microengineering, 1992. 2(4): p. 225-228.
12. Dechev N., W.L. Cleghorn, and J.K. Mills. *Microassembly of 3-D MEMS Structures Utilizing a MEMS Microgripper with a Robotic Manipulator*. in *International Conference on Robotics &Automation*. 2003. Taipei, Tsiusn.
13. Thompson J.A. and R.S. Fearing. *Automating Microassembly with Ortho-tweezers and Force Sensing*. in *IROS 2001*. 2001. Maui, HI.
14. Tsui K., et al., *Micromachined end-effector and techniques for directed MEMS assembly.* Journal of Micromechanics and Microengineering, 2004. 14: p. 542-549.
15. Prasad R., K.-F. Bohringer, and N.C. MacDonald. *Design, fabrication, and characterization of single crystal silicon latching snap fasteners for micro assembly*. in *Proc. ASME Int. Mech. Eng. Congress and Exposition (IMECE'95)*. 1995. San Francisco, CA.

16. Milanovic´ V., *Multilevel Beam SOI-MEMS Fabrication and Applications.* Journal of Microelectromechanical Systems, 2004. 13(1): p. 19-30.
17. Hollar S., et al. *Robot leg motion in a planarized SOI/2-poly process*. in *Hilton Head 2002 workshop*. 2002. Hilton Head Island, S.C.
18. Last M.E., *Pick and Place Silicon on Insulator Microassembly*, in *Electrical Engineering and Computer Science*. 2005, PhD Thesis, University of California, Berkeley: Berkeley.
19. Kruglick E.J.J., *Microrelay design, performance, and systems*, in *Engineering - Electrical Engineering and Computer Science*. 1999, PhD Thesis, University of California, Berkeley: Berkeley.
20. Dechev N., W.L. Cleghorn, and J.K. Mills, *Microassembly of 3-D microstructures using a compliant, passive microgripper.* Journal of Microelectromechanical Systems, 2004. 13(2): p. 176-189.
21. Skidmore G., et al. *Assembly technology across multiple length scales from the micro-scale to the nano-scale*. in *17th International Conference on MEMS*. 2004.
22. Shimada E., et al. *Prototyping Millirobots using Dextrous Microassembly and Folding*. in *Proc. ASME IMECE/DSCD*. 2000. Orlando Florida.
23. *Applied Microstructures* http://appliedmst.com/technology.html
24. Garmire D., R.S. Muller, and J. Demmel. *Vision-based teleoperation of a stroboscopic microscopic interferometric system for remote dynamic MEMS testing*. in *IEEE/LEOS International Conference on Optical MEMS and Their Applications*. 2005.
25. Brosnihan T.J., et al. *Embedded interconnect and electrical isolation for high-aspect-ratio, SOI inertial instruments*. in *International Conference on Solid State Sensors and Actuators. Transducers '97*. 1997. Chicago.
26. Sinclair M.J. *A High Force Low Area MEMS Thermal Actuator*. in *2000 Inter Society Conference on Thermal and Thermomechanical Phenomena*. 2000. Las Vegas, NV.
27. Zhou L., J.M. Kahn, and K.S.J. Pister, *Scanning micromirrors fabricated by an SOI/SOI wafer-bonding process.* Journal of Microelectromechanical Systems, 2006. 15(1): p. 24-32.
28. Jang D.-S. and D.E. Kim, *Optimum film thickness of thin metallic coatings on silicon substrates for low load sliding applications.* Tribology International, 1996. 29(4): p. 345-356.
29. Dario P., et al., *REVIEW Microactuators for microrobots: a critical survey.* Journal of Micromechanics and Microengineering, 1992. 2: p. 141-157.
30. Mohebbi M.H., et al. *Omnidirectional Walking Microrobot Using MEMS Thermal Cilia Arrays*. in *ASME International Mechanical Engineering Congress and Exposition (IMECE'01)*. 2001. New York, NY.
31. Ebefors T., et al. *A Walking Silicon Micro-robot*. in *10th Int. Conference on Solid-State Sensors and Actuators (Transducers 99)*. 1999. Sendai, Japan.
32. Hollar S., et al. *Solar Powered 10 mg Silicon Robot*. in *MEMS 2003*. 2003. Kyoto, Japan.
33. B.R.Donald et al., *An Untethered, Electrostatic, Globally Controllable MEMS Micro-Robot.* Journal of Microelectromechanical Systems, 2006. 15(1).

34. Kunkel D., *Spider Spinneret* http://www.astrographics.com/GalleryPrintsIndex/GP2017.html
35. Yeh R., S. Hollar, and K.S.J. Pister. *Single mask, large force, and large displacement electrostatic linear inchworm motors*. in *The 14th IEEE International Conference on Micro Electro Mechanical Systems. MEMS 2001.* 2001.
36. Hollar S., S. Bergbreiter, and K.S.J. Pister. *Bidirectional Inchworm Motors and Two-DOF Robot Leg Operation*. in *Transducers 2003*. 2003. Boston.
37. Zhou L., et al. *Two-Axis Scanning Mirror for Free-Space Optical Communication between UAVs*. in *2003 IEEE/LEOS International Conference on Optical MEMS*. 2003. Waikoloa, HI.